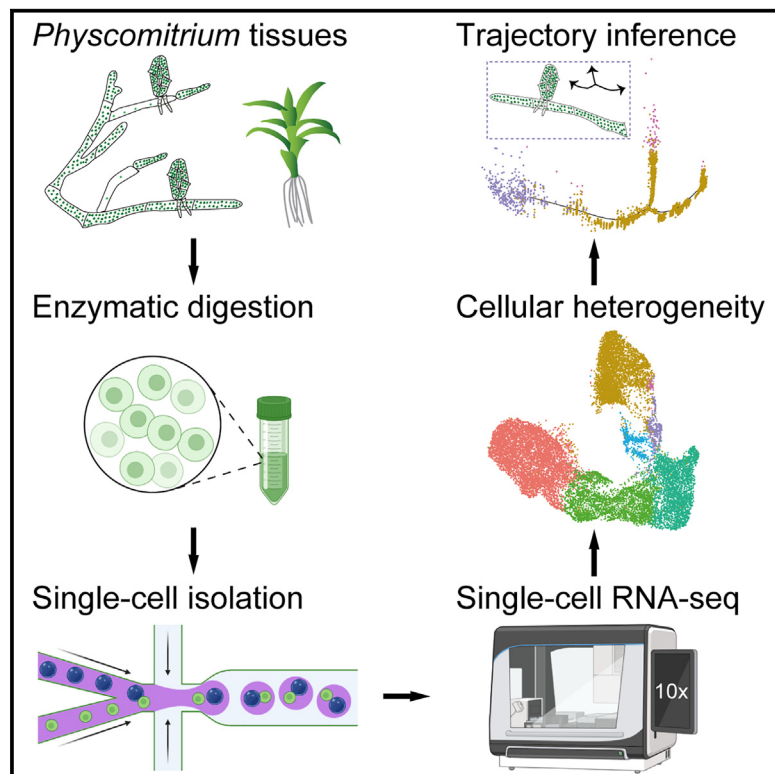


Single-cell RNA sequencing reveals dynamics of gene expression for 2D elongation and 3D growth in *Physcomitrium patens*

Graphical abstract



Authors

Zexi Chen, Wenbo Wang,
Shizhao Zhou, ..., Xuwu Sun,
Heqiang Huo, Li Liu

Correspondence

liuli2020@hubu.edu.cn

In brief

Chen et al. perform transcriptomic analyses on *Physcomitrium patens* across two-dimensional (2D) and 3D growth, generating a single-cell atlas composed of the chloronema, caulinema, tip cell, bud, and gametophore. The inference of developmental trajectories for 2D tip elongation and 3D bud differentiation provides a valuable resource for future investigations.

Highlights

- A reference cell atlas for bryophytes is generated by scRNA-seq
- Major cell types and marker genes are identified in *P. patens*
- The trajectory of 2D-to-3D growth transition is built at single-cell resolution
- scRNA-seq co-expression network identifies candidate auxin-associated genes



Article

Single-cell RNA sequencing reveals dynamics of gene expression for 2D elongation and 3D growth in *Physcomitrium patens*

Zexi Chen,^{1,5} Wenbo Wang,^{1,5} Shizhao Zhou,^{2,5} Lulu Ding,¹ Zhanwu Xu,¹ Xuwu Sun,³ Heqiang Huo,⁴ and Li Liu^{1,6,*}

¹State Key Laboratory of Biocatalysis and Enzyme Engineering, Hubei Collaborative Innovation Center for Green Transformation of Bio-Resources, Hubei Key Laboratory of Industrial Biotechnology, School of Life Sciences, Hubei University, Wuhan 430062, China

²CAS Key Laboratory for Plant Diversity and Biogeography of East Asia, Kunming Institute of Botany, Chinese Academy of Sciences, Kunming, Yunnan 650201, China

³National Key Laboratory of Cotton Bio-breeding and Integrated Utilization, State Key Laboratory of Crop Stress Adaptation and Improvement, Key Laboratory of Plant Stress Biology, School of Life Sciences, Henan University, 85 Minglun Street, Kaifeng 475001, China

⁴Mid-Florida Research and Education Center, Department of Environmental Horticulture, University of Florida, 2725 South Binion Road, Apopka, FL 32703, USA

⁵These authors contributed equally

⁶Lead contact

*Correspondence: liuli2020@hubu.edu.cn

<https://doi.org/10.1016/j.celrep.2024.114524>

SUMMARY

The transition from two-dimensional (2D) to 3D growth likely facilitated plants to colonize land, but its heterogeneity is not well understood. In this study, we utilized single-cell RNA sequencing to analyze the moss *Physcomitrium patens*, whose morphogenesis involves a transition from 2D to 3D growth. We profiled over 17,000 single cells covering all major vegetative tissues, including 2D filaments (chloronema and caulinema) and 3D structures (bud and gametophore). Pseudotime analyses revealed larger numbers of candidate genes that determine cell fates for 2D tip elongation or 3D bud differentiation. Using weighted gene co-expression network analysis, we identified a module that connects β -type carbonic anhydrases (β CAAs) with auxin. We further validated the cellular expression patterns of β CAAs and demonstrated their roles in 3D gametophore development. Overall, our study provides insights into cellular heterogeneity in a moss and identifies molecular signatures that underpin the 2D-to-3D growth transition at single-cell resolution.

INTRODUCTION

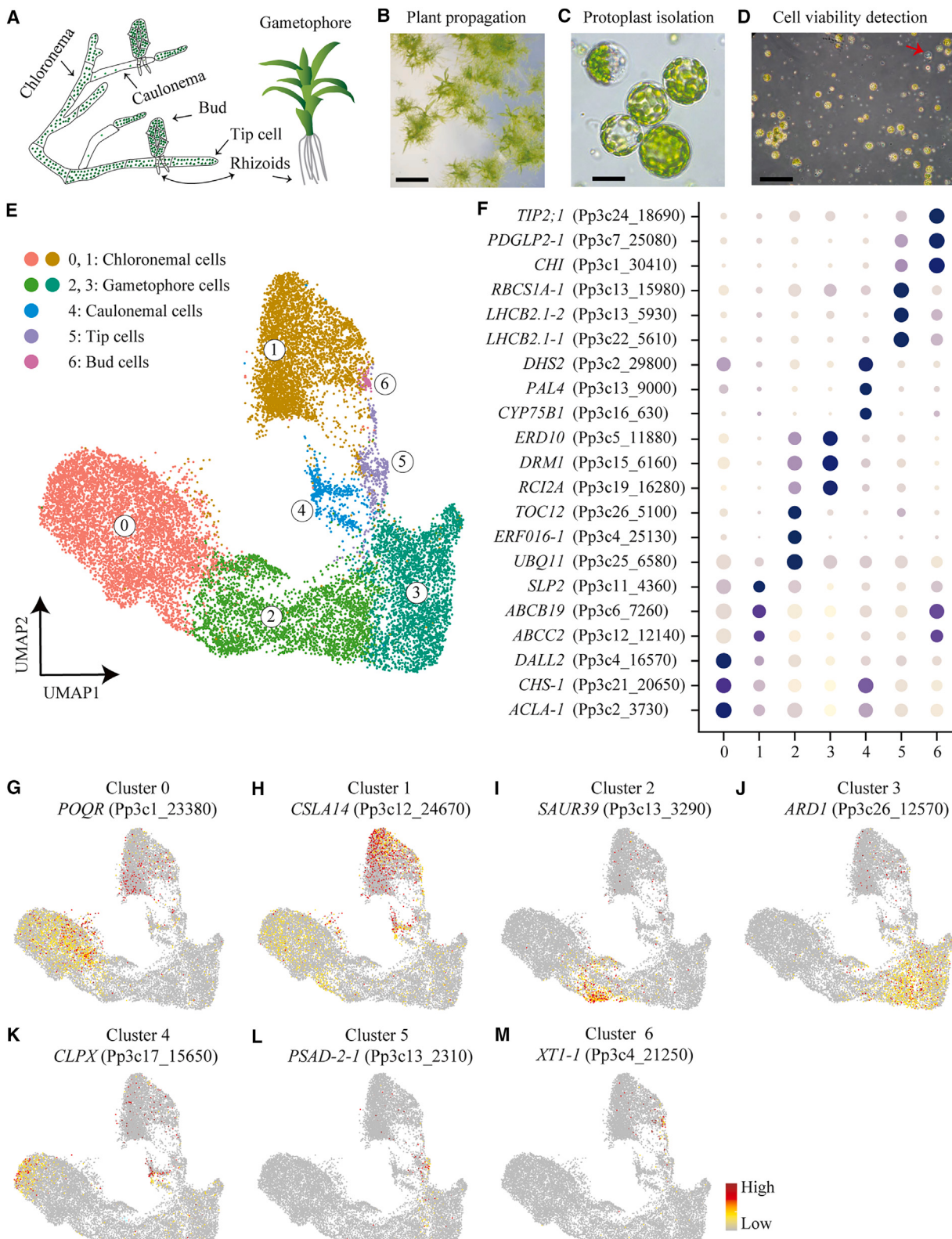
The colonization of land by plants facilitated adaptive evolution and morphological innovations.^{1–4} These included enhanced tolerance to abiotic stresses as well as advancements in embryogenesis and vascular development. One of these innovations, the three-dimensional (3D) patterning, likely played a crucial role in facilitating this colonization and shaping the terrestrial landscape of land plants (embryophytes). Bryophytes, comprising mosses, hornworts, and liverworts, are non-vascular plants that initiated the terrestrial colonization process approximately 450 million years ago.⁵ In angiosperms, the transition from 2D to 3D growth occurs during embryo development, and disrupting this process can be lethal.² In contrast, the moss *Physcomitrium* (formerly *Physcomitrella*) *patens* undergoes a 2D protonemal phase, consisting of chloronemata and caulinemata, before transition to 3D growth.^{6,7} Interestingly, the protonemata can be propagated indefinitely through 2D tip growth before forming 3D buds, an early stage of gametophore development.^{8,9} Therefore, *P. patens* serves as an ideal system for inves-

tigating the molecular mechanisms underlying the transition from 2D to 3D growth in plants.

P. patens can generate multiple types of stem cells across its life cycle.¹⁰ For example, both chloronemal and caulinemal cells possess self-renewal capacity and can differentiate into each other via tip growth.² The distinct fates of these cells may depend on their cellular auxin activity or responsiveness.¹¹ During caulinema development, side-branch cells initiate through division on two planes, with approximately 5% transitioning into buds.¹² Additionally, buds can also originate from side branches of secondary chloronemal cells,¹¹ demonstrating that the ability to initiate 3D growth exists in both chloronemata and caulinemata. In contrast to the 2D-tip elongation, the apical stem cell in a bud expands through diffuse growth and undergoes four asymmetric divisions to establish a tetrahedral form.⁶ This configuration is crucial for promoting growth on three planes and is a requisite for the formation of a mature 3D gametophore.

In the past 15 years, an increasing number of genes have been identified to play important roles in the cell developmental processes of 2D tip growth or 3D transition in *P. patens*. For





(legend on next page)

example, genes from class XI myosin (*myoXla*), Rho of plants (ROP) GTPase (*ROP1*), and RAB GTPase (*Rab-E14*), are involved in polarized transport and play essential roles in tip growth or branching by controlling cell division.^{13–15} Several genes related to bud formation and gametophore development have also been identified, such as *AINTEGUMENTA*, *PLETHORA*, and *BABY BOOM* (*APB*); *DEFECTIVE KERNEL 1* (*DEK1*); *CLAVATA3-like* (*CLE*) and *RECEPTOR-LIKE PROTEIN KINASE 2* (*RPK2*); *NO GAMETOPHORES 1* (*NOG1*); and *NO GAMETOPHORES 2* (*NOG2*).^{12,16–19}

Functioning similarly as their *Arabidopsis* homologs, moss *CLE1–CLE7* and *RPK2* not only influence plane orientation during bud cell division but also regulate protonemal stem cell activity or identity by modulating auxin homeostasis.^{18,20} *NOG1* and *NOG2* both act as positive regulators of bud formation and cell division during the establishment of 3D growth,^{17,19} whereas *DEK1* negatively modulates bud formation but positively controls the cell division plane.¹⁶ Coincidentally, *NOG2* has also been shown to encode a hydroxycinnamoyl transferase (HCT), and their homologs are highly conserved among embryophytes.²¹ The morphological innovation of 3D patterning in moss may have synchronized with the emergence of these genes, but the detailed regulatory mechanisms remain obscure.

In a previous study by Frank and Scanlon,²² the tip and bud cells were microdissected for transcriptomic analyses, revealing molecular signatures specific to each cell type. This approach has facilitated deciphering the potential genetic mechanisms responsible for developmental differences. Numerous regulators participating in cell wall biogenesis, hormone signaling, cytoskeleton, asymmetric cell division, and photosynthesis were identified. These genes may serve as key signatures for distinguishing the tip and bud cells. Nevertheless, the morphological resemblance between newly initiated bud cells and tip cells poses a challenge to the microdissection method, limiting the ability to comprehensively characterize the molecular signatures of these cell types.

Single-cell RNA sequencing (scRNA-seq) has been used extensively to profile molecular signatures across various cell types in angiosperms.^{23,24} However, no studies have explored cell differences using a single-cell atlas in mosses to date. Here, we employed scRNA-seq to identify the potential signatures of distinct cell types from 2D to 3D growth phases in *P. patens*. Our analysis identified seven heterogeneous clusters, which were partitioned into five distinct cell types. In combination with pseudotime analyses, we reconstructed the developmental trajectories of tip growth and bud differentiation at the

cell-type level. The hundreds of identified marker genes serve as a valuable resource for research on plant 3D patterning.

RESULTS

scRNA-seq and cell clustering of *P. patens*

The vegetative tissues of *P. patens* exhibit characteristics consisting of both 2D and 3D growth forms.² These include the protonemata, buds, and leafy gametophores, which are co-developed by multiple cell populations. To decipher the gene expression patterns in different lineage cells during 2D and 3D development, we selected 14-day-old cultures after protonema propagation to isolate protoplasts for scRNA-seq using the 10x Genomics platform (Figures 1A–1C and S1). The cells were confirmed by viability assessment with a threshold of >85% and diameter measurement with a threshold of <40 μm (Figure 1D; Table S1).

Initially, a total of 21,269 cells from three biological replicates (Rep1–Rep3) were individually mixed with the single-cell reaction reagents to construct cDNA libraries for sequencing. Following stringent quality control at both the cell and gene levels, a refined dataset from 17,849 cells was used for further analysis (Figure S2; Table S2). The data clusters from the three replicates aligned well when analyzed using either *t*-distributed stochastic neighborhood embedding or uniform manifold approximation and projection (UMAP) methods (Figure S3). Consequently, all data were combined into a single dataset for subsequent cell clustering and annotation. The analysis revealed approximately a median of 15,760 unique molecular identifiers per cell, 3,727 expressed genes per cell, and more than 23,800 total genes detected in the population (Table S2).

Utilizing Seurat v4.3.0, we partitioned the cells into seven transcriptionally distinct clusters, which were then visualized by 2D UMAP plots (Figure 1E). The percentage of cells in each cluster ranged from 0.36% to 35.09% (Table S3). We subsequently identified sets of cluster-enriched genes (CEGs) that were enriched or specific to particular clusters (Figure 1F; Table S4). Due to the scarcity of marker genes for cell types, we compared our data with two earlier datasets of tissue and cell-specific transcriptomes in *P. patens*: one generated with microarrays for multiple tissues and another with RNA-seq for tip- and bud-growing cells.^{22,25} First, by comparing our data with the microarray datasets, we found that many CEGs from this study were predominantly expressed in chloronemata (clusters 0 and 1), caulinemata (cluster 4), and gametophores (clusters 2 and 3) (Table S5). Second, a comparison with the RNA-seq datasets

Figure 1. Overview of the 10x Genomics scRNA-seq application in the moss *P. patens*

- (A) Diagram of 2D and 3D growth phases, including chloronema (with numerous chloroplasts), caulinema (with fewer or poorly developed chloroplasts), tip cell, bud, leafy gametophore, and rhizoids (rooting structures).
- (B) Sampling stage of tissues after propagation. Scale bar: 3 mm.
- (C) Single-cell protoplasts isolated via enzymatic digestion of tissues. Scale bar: 20 μm.
- (D) Detection of cell viability using trypan blue staining. About 660 protoplasts were used for counting. A red arrow indicates the dead protoplast. Scale bar: 100 μm.
- (E) UMAP visualization of 7 cell clusters in *P. patens*. Colors indicate distinct cell clusters. Each dot represents a single cell. $n = 17,849$ cells.
- (F) Expression patterns of significantly enriched genes in each cluster. Three genes are shown for each cluster, with gene symbols of their *Arabidopsis* homologs displayed on the left. Dot diameter and color denote the proportion of cells and the average expression level of the respective gene. See also Table S4.
- (G–M) UMAP expression patterns of the representative marker genes for each cell cluster. The gene symbols of their *Arabidopsis* homologs were displayed. Color bar denotes relative expression level. Each dot represents a single cell. See also Figures S4–S10 and Table S5.

revealed that some CEGs showed high expression in tip (cluster 5) or bud (cluster 6) cells (Table S5). UMAP visualization showed that these putative tissue or cell-type marker genes consistently exhibited high or specific mean expression across clusters (Figures 1G–1M and S4–S10). For instance, cells in clusters 5 and 6 exhibited high expression of genes related to photosynthesis and cell wall biogenesis/metabolism, respectively (Figures 1L, 1M, S9, and S10; Table S5). However, the rhizoids, emerging from epidermal cells at the base of gametophores,²⁶ could not be recognized in this study by tissue-enriched genes (Figure S11; Table S5).

Intriguingly, the clusters 0 and 1, representing chloronemal cells, were scattered on the UMAP plot, whereas the clusters 2 and 3, representing gametophore cells, were situated adjacent to each other (Figure 1E). This observation suggested the presence of at least two distinct types of chloronemal cells with unexpected heterogeneity. Additionally, the bud cells were positioned closely to the chloronemal cells of cluster 1 but distinctly separated from other cell types, such as tip cells, caulonemal cells, and gametophore cells. Overall, these unsupervised analyses provided a detailed profile of the cellular heterogeneity within 2D and 3D tissues of *P. patens*.

Validation of cluster identities by representative markers

To further assign cell types to specific clusters, we selected a series of CEGs to generate promoter reporter lines (Figure 2; STAR Methods). One of the genes enriched in cluster 0, *Pp3c2_7150*, a homolog of *Arabidopsis JMD5*,²⁷ was preferentially expressed in chloronemal cells with multiple side branches (Figures 2A and 2B; Table S4). Interestingly, the cluster 1-enriched gene *Pp3c16_17510*, a homolog of *CRPK1* protein kinase,²⁸ was predominantly expressed in the elongated chloronemal filaments that had only a few side-branch initiations (Figures 2C and 2D; Table S4). Therefore, clusters 0 and 1 likely represented the distinct tip-growing patterns by side branching and apical extension during protonemal outgrowth.⁷

Intriguingly, as one of the mammalian *EYES ABSENT* (*EYA*) homologs,²⁹ the cluster 2-enriched gene *Pp3c1_31250* showed high expression both in the stem and mid-stem leaves rather than in apical leaves (Figures 2E and 2F; Table S4). Additionally, the cluster 3-enriched gene *Pp3c5_21160*, a homolog of *Arabidopsis OST1*,³⁰ was also expressed in the gametophore stem but almost undetectable in mid-stem leaves (Figures 2G and 2H; Table S4). However, strong promoter activity of this gene was predominantly detected in apical leaves. Therefore, clusters 2 and 3 appeared to represent the cells with preferential expression patterns in mid-stem and apical leaves, respectively.

Reporter assays further revealed that the cluster 4-enriched gene *Pp3c22_12740*, a homolog of *Arabidopsis KUP3* that may be involved in K⁺ uptake,³¹ was highly expressed in caulonemal cells derived from chloronemal branching (Figures 2I and 2J; Table S4). One of the cluster 5-enriched photosynthetic genes, *Pp3c3_14080* (*PSBO2-1*), was mainly expressed in tip-growing cells rather than non-tip cells derived from chloronemata (Figures 2K and 2L; Table S4). Moreover, the cluster 6-specific enriched gene *Pp3c16_25600*, a homolog of *Arabidopsis* phosphate transporter *PHT2;1*,³² was highly expressed in bud cells

but undetectable in neighboring chloronemal cells (Figures 2M and 2N; Table S4). Taken together, these expression patterns of the representative genes validated our predicted cluster identities.

Characterization and functional annotation of cell clusters

A total of 2,691 enriched CEGs were identified, with the number of genes in each cluster ranging from 187 to 799 (Tables S3 and S4). The highest proportion of CEGs (29.69%) was found in bud cells (cluster 6), while the lowest (6.95%) was observed in caulonemal cells (cluster 4). Interestingly, although the bud tissue comprised the smallest proportion of cells, it contained the highest number of CEGs. Furthermore, while the tip cells (cluster 5) had a proportion of cells similar to caulonemal cells, they exhibited nearly three times the number of CEGs (Table S3).

Next, we compared the number of unique and shared CEGs across different cell clusters. Surprisingly, the chloronemal cell clusters 0 and 1 shared only one CEG (*Pp3c25_10190*), which is homologous to the *Arabidopsis* cinnamate-4-hydroxylase-encoding gene *C4H*, a regulator in the phenylpropanoid pathway that impacts auxin transport (Figures 3A and S12A).³³ Even though gametophore cell clusters 2 and 3 shared 34 CEGs, it comprised a very low proportion (34 of 899, 3.78%) of the total, suggesting that specific functions might be associated with the heterogeneous cells within the same tissues. Interestingly, chloronemal and gametophore cells shared only 9 CEGs, accounting for less than 0.50% (9 of 1,821) of the total. In contrast, some tissues shared a substantial number of CEGs, such as 281 between chloronemal (primarily in cluster 1) and bud cells, 198 between gametophore (primarily in cluster 3) and tip cells, and 73 between tip and bud cells (Figures 3B, S12B, and S12C). However, relatively few CEGs were shared across three or more tissue types. In addition, we screened a total of 60 CEGs encoding transcription factors across these cell types, including 2 shared genes: *Pp3c22_5440* (*BBX16*) between clusters 1 and 6 and *Pp3c2_23590* (*WRKY3*) between clusters 3 and 5 (Figure S13; Table S6). Surprisingly, despite the remarkable transcriptional reprogramming in tip and bud cells, each was enriched for only 2 transcription factors.

To elucidate the characteristics of distinct cell clusters, we performed Gene Ontology (GO) analyses (adjusted *p* < 0.05) of CEGs (Figures 3C–3I; Table S7). Notably, the GO analysis aligned with the heterogeneity observed in subpopulations of chloronemal cells. Cluster 0 was characterized by terms related to small molecule biosynthesis and hormonal regulation, whereas the genes enriched in cluster 1 were predominantly associated with transmembrane transport and cell wall organization/biogenesis (Figures 3C and 3D). Similarly, distinct signatures were observed for the two gametophore sub-cell types. Cluster 2 was largely marked by genes involved in stress response, while the genes enriched in cluster 3 were associated with translation and photosynthesis (Figures 3E and 3F). Specifically, genes associated with phenylpropanoid or secondary metabolite biosynthesis were significantly enriched in cluster 4 (caulonemal cells) (Figure 3G). In contrast, cluster 5 (tip cells) exhibited processes related to photosynthesis, translation, and cytokinin response (Figure 3H). Likewise, the GO terms

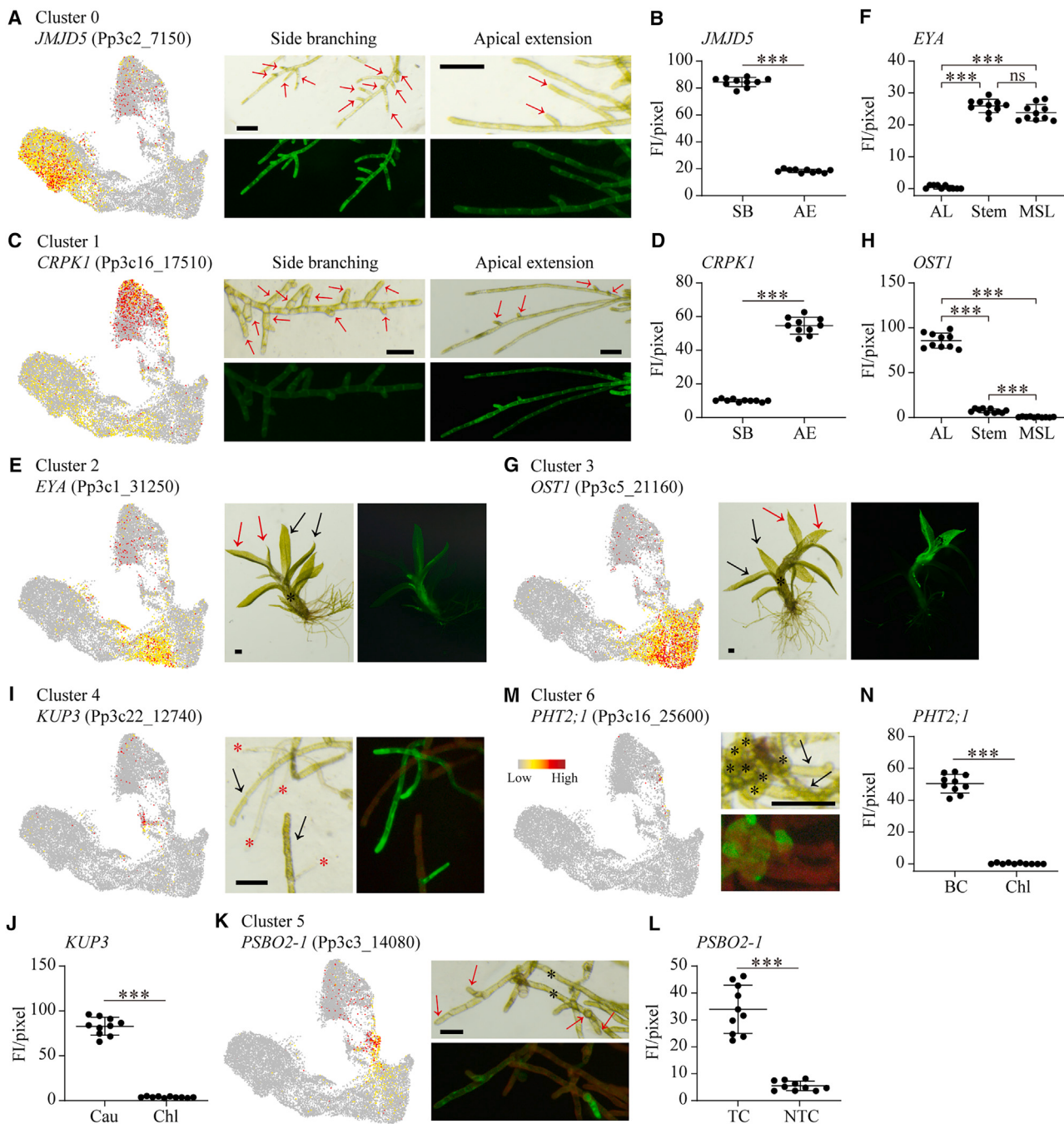
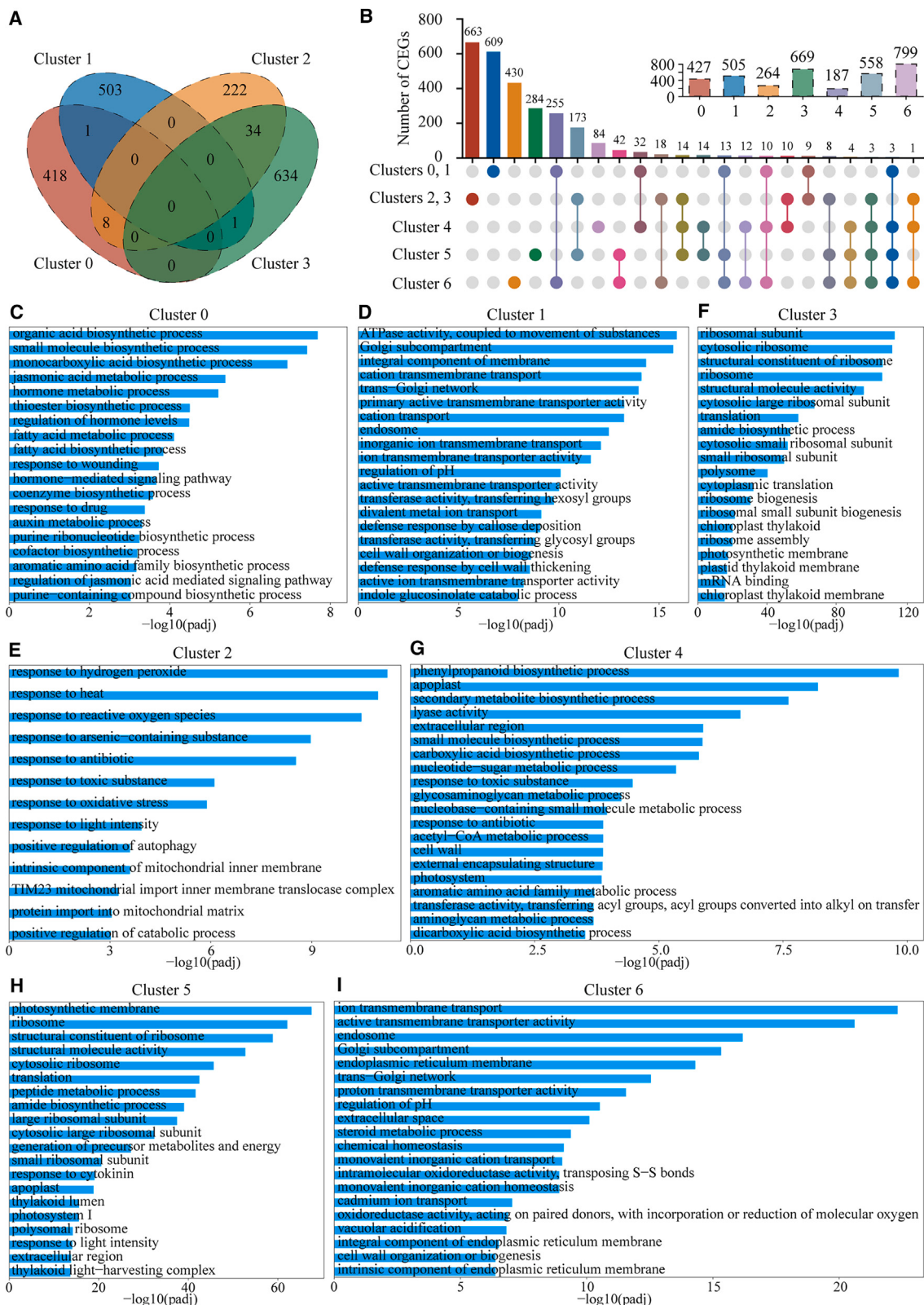


Figure 2. Expression of cell-type representative marker genes

(A, C, E, G, I, K, and M) For each cluster, UMAP visualization of the representative gene (left) and expression pattern of the promoter with EGFP reporter *in planta* (middle or right) (STAR Methods). Scale bars: 125 μ m. In (A and C), photographs show distinct tip-growing patterns by side branching and apical extension. Arrows denote the side branches emerging from chloronemal filaments. In (E and G), expression patterns of the representative genes in gametophores can be seen. Black and red arrows denote the mid-stem and apical leaves, respectively. Asterisks indicate the stems of the gametophores. In (I), asterisks and arrows denote the caulinemal and chloronemal cells, respectively. In (K), arrows and asterisks denote the tip-growing and non-tip cells, respectively. In (M), asterisks and arrows denote the bud and chloronemal cells, respectively.

(B, D, F, H, J, L, and N) The fluorescence intensity (FI) of GFP was quantified with ImageJ. Values are the means \pm SD ($n = 10$ images). Student's t test, *** $p < 0.001$. ns, no significant difference. SB, side branching; AE, apical extension; AL, apical leaf; MSL, mid-stem leaf; Cau, caulinemal cell; Chl, chloronemal cell; TC, tip cell; NTC, non-tip cell; BC, bud cell.



(legend on next page)

associated with transmembrane transport and cell wall organization/biogenesis were prominently enriched in cluster 6 (bud cells) (Figure 3I). Interestingly, we observed that clusters 1 and 6 both showed enrichment related to the indolebutyric acid (an auxin precursor) response (Table S7),³⁴ indicating a common hormonal signal during the chloronemal apical extension and bud growth.

Reconstruction of the trajectories of 2D tip elongation and 3D bud differentiation

Since side-branch initial cells in 2D protonemata can either undergo self-renewal through tip elongation or differentiate to form 3D buds,^{2,11} scRNA-seq offers a method for exploring the developmental trajectories of these two processes. UMAP analysis revealed that the clusters 5 and 6 corresponding to tip and bud cells were closest to cluster 1 of chloronemata (Figures 1E and 4A). In addition, our data showed that transcripts of the tip growth-related genes *myoXla*, *Rab-E14*, and *ROP*^{13–15} were primarily detected in clusters 1 and 5 (Figures 4B, 4C, and S14A–S14F). Likewise, we found that the protonema-specific genes (*RM09* and *RM55*)³⁵ and several bud development-related genes (*APB3*, *DEK1*, *NOG1*, *CLE7*, and *RPK2*)^{12,16–18} were all predominantly expressed in cluster 1 (Figures S14G–S14M). Consistent with previously published data,²⁰ the expression of two CLAVATA pathway-related genes, *CLE7* and *RPK2*, was also detected in the tip cells (Figures 4D and 4E). Interestingly, they exhibited a higher transcript abundance in cluster 1 than in cluster 5, indicating its physiological significance. These results demonstrate that the distribution patterns of tip- or bud-related genes in clusters 1, 5, and 6 from our scRNA-seq profiles coincided with published data.

To reconstruct trajectories of tip growth or bud differentiation, we employed the Monocle 2 algorithm.^{36,37} Interestingly, cells from cluster 1 were sorted into three distinct trajectories (named branches 1–3) (Figure 4F; Table S8). Two of these branches were grouped with the cells of clusters 5 and 6 during the early pseudotime stages, respectively. We found that the gene *myoXla* was predominantly expressed at the branch point and in the later stage of cluster 5 along branch 2 (Figure 4G). In contrast, the *RPK2* exhibited elevated expression in cluster 6 at a later stage of branch 3 compared to its relatively low abundance in the tip elongation trajectory (Figure 4L). The integrated heatmap and associated functional annotations illustrated that the pseudotime trajectories of clusters 5 and 6 were associated with numerous genes involved in photosynthesis and cell wall biogenesis/modification, respectively (Figure 4Q; Tables S9 and S10). For instance, photosynthesis genes such as *Pp3c6_1620* (*PSAD-2-2*) and *Pp3c4_17240* (*LHCB2.1-3*) were actively transcribed at the later stage of branch 2 (Figures 4J and S15D). In addition, two CO₂-concentrating mechanism (CCM)-related genes, the β-type carbonic anhydrases *βCA2* and *βCA6*, which are implicated in inorganic carbon uptake in *P. patens*,³⁸ exhibited high expression during the tip elongation

trajectory (Figures 4I and 4K). Conversely, cell wall-related genes such as *Pp3c19_18770* (*SBT1.7*), *Pp3c8_870* (*EXPA1*), and *Pp3c25_4070* (*XTH9-2*) showed increased expression over the course of bud growth in pseudotime (Figures 4N and 4Q).

Since auxin is known to stimulate bud formation,¹¹ we hypothesized that increased activity in auxin transport/biosynthesis might play a role in the transition from 2D to 3D growth. Supporting this hypothesis, the genes *Pp3c23_680*, *Pp3c1_2170*, and *Pp3c14_22450*, whose homologs in *Arabidopsis* encode amino-phospholipid ATPase (*ALA11*), pyrophosphatase (*AVP1*), and cyclopropyl isomerase (*CPI1*), required for auxin polar transport or auxin-mediated development,^{39–41} were highly expressed at the later stages of branch 3 (Figures 4Q and S15A–S15C). Moreover, the expression of *Pp3c10_2340*, homologous to transmembrane kinase 1 (*TMK1*), a key regulator in auxin signaling,⁴² also increased alongside with bud differentiation (Figures 4O and 4Q). In contrast to a simple extension of tip growth, bud initiation undergoes multiple asymmetric divisions on a 3D plane to form a tetrahedral shape,⁶ suggesting a more complex molecular mechanism. Indeed, several genes, such as *Pp3c24_6930* (*DGL1*), *Pp3c7_5350* (*LCB1*), and *Pp3c2_13410* (*PAS2*), whose *Arabidopsis* homologs regulate the cell differentiation/division/expansion,^{43–45} were highly expressed at the later stages of branch 3 (Figure 4Q; Table S10). We also found a highly related bud differentiation trajectory gene, *Pp3c14_3360*, encoding a heat shock protein (Figure 4P). Its homolog, *SHD*, is involved in meristem cell division via the activation of CLAVATA proteins in *Arabidopsis*.⁴⁶ These molecular signatures suggest that the 3D bud differentiation may be co-regulated by multiple processes, including cell wall biogenesis, auxin transport and signaling, and cell expansion or division, whereas 2D tip growth is mainly promoted by enhanced photosynthesis capacity.

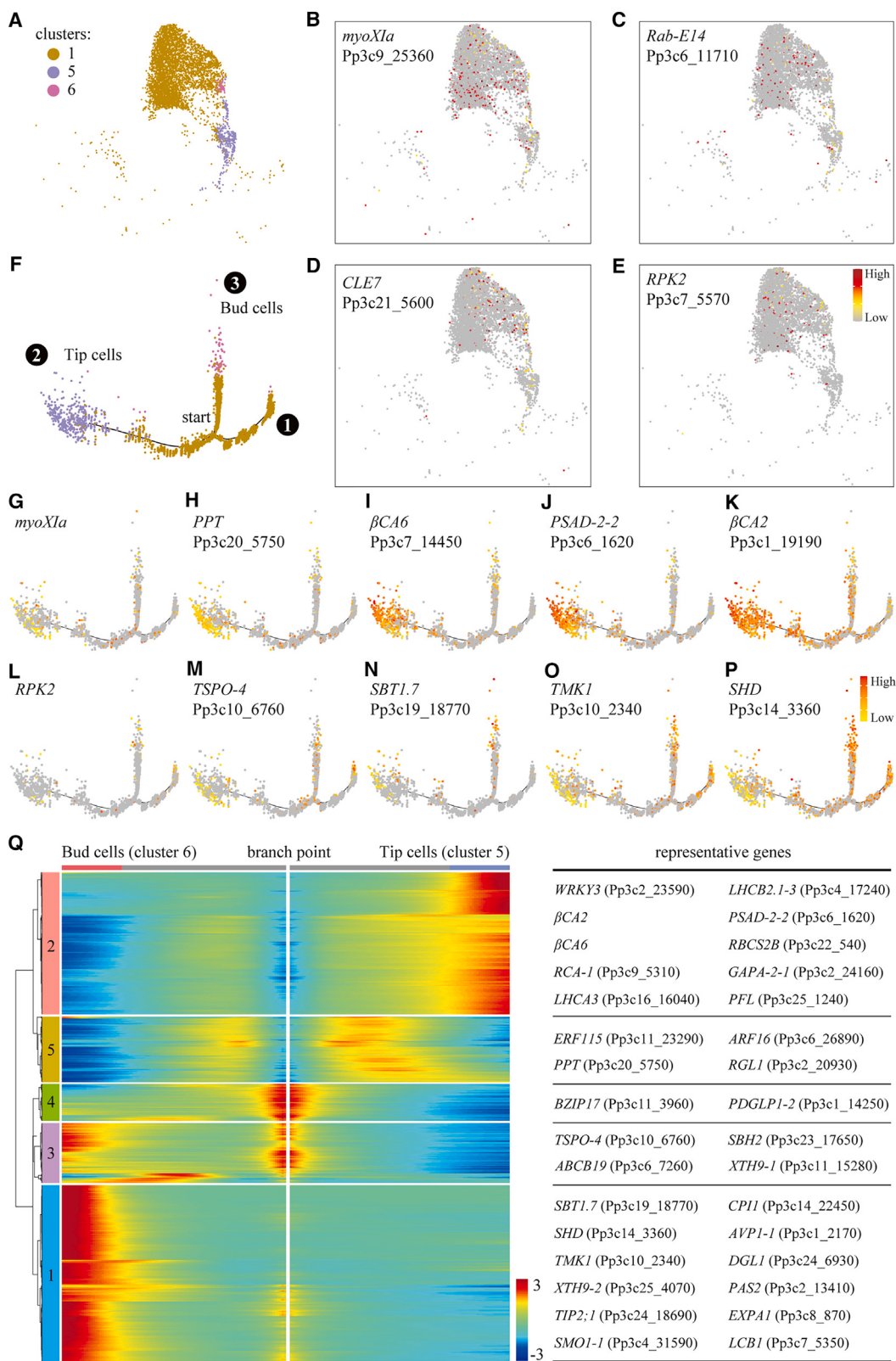
Roles of auxin in various cell types

To further investigate the roles of auxin in distinct cell types, we examined the UMAP expression patterns of tryptophan (Trp) aminotransferase (TAR) genes, which are of interest because auxin is mainly derived from a Trp-dependent biosynthetic pathway.⁴⁷ In *P. patens*, we observed that *TARA* and *TARC* were the predominantly expressed TAR genes (Figures 5A–5D), consistent with previous findings.⁴⁸ The UMAP clusters showed that only *TARA* exhibited relatively high expression levels, with its enrichment in cluster 1 of chloronemal cells (Figure 5A; Table S4); however, its transcripts were only slightly detected in other cell types, such as bud and gametophore cells. Conversely, the expression of *TARC* was generally low and mainly observed in chloronemal cells (cluster 1) and gametophore cells (cluster 3) (Figure 5C). These results demonstrate that Trp-dependent auxin biosynthesis may be most active in chloronemal cells, particularly in cluster 1.

Gretchen Hagen 3 (*GH3*) was originally isolated for auxin responsiveness in soybean.^{49,50} Later studies revealed that the *GH3* family encodes acyl acid amido synthetases, which have

Figure 3. Venn analyses of CEGs and GO term annotations

- (A) Venn diagram showing the number of shared or unique CEGs among clusters 0–3.
- (B) Upset plots illustrating the number of shared or unique CEGs across different clusters/tissues. See also Table S4.
- (C–I) GO term analyses of CEGs from each cell cluster. The top 20 terms of each cluster are shown. See also Table S7.



(legend on next page)

a conserved function in regulating auxin homeostasis by forming indole-3-acetic acid (IAA)-amide conjugates.^{51–53} We found that *GH3-1* in *P. patens* showed a broad expression pattern across all analyzed cell types, with significant enrichment in cluster 0 of chloronemal cells (Figure 5E; Table S4). By contrast, another homolog, *GH3-2*, exhibited a more restricted expression to a subset of cells in clusters 1, 3, 4, and 5 (Figure 5F). Interestingly, *TARA* and *GH3-1* were individually enriched in different clusters of chloronemal cells, suggesting that biosynthesis of active IAA and storage of inactive IAA-amide conjugates may be controlled by distinct sub-cell types. Moreover, the expression of *GH3-1* indicates that IAA-amide conjugates might be widespread in multiple cell types, potentially serving as a reservoir for rapidly releasing active IAA without requiring *de novo* biosynthesis.

The soybean *GmGH3* promoter has been effectively utilized in *P. patens* to study auxin distribution and sensing.^{54,55} To determine cell heterogeneity and auxin responsiveness in different developing cells, such as 2D tip or 3D bud cells, we examined the expression of the reporter *pGmGH3::EGFP* in *planta*. We labeled the cluster 0-type cells 1–6 (C1–C6) from tip to base along the axis of chloronemal growth and found that the reporter activity was notably elevated in C1 compared to side-branched cells (Figure 5G). Moreover, the tip-linked C2 exhibited signals nearly identical to C1, while reporter activities gradually diminished from C3–C6 along the primary growth extension. This pattern might result from the inhibitory effect of auxin on chloronemal branching.¹¹ In contrast to the chloronemata, auxin responsiveness varied during the growth or differentiation of caulinemata. The reporter activities were relatively high in side-branch initial cells (Figure 5H), which can subsequently differentiate into buds, chloronemata, or caulinemata.¹¹ Interestingly, subapical caulinemal cells showed lower *pGmGH3::EGFP* activities, whereas the mature side branch caulinemal cells displayed higher responsiveness, indicating a dual role in auxin on differentiation and cell identity maintenance of caulinemata. Moreover, our observations showed that reporter activities were highly distributed throughout the whole bud tissue (Figure 5I). Further examinations uncovered that the gametophore growth was accompanied by an uneven distribution of *pGmGH3::EGFP* activities, which were predominantly concentrated at the apex, stem, and rhizoids (Figure 5J). These findings demonstrate the divergent patterns of auxin responsiveness across the 2D-to-3D growth of *P. patens*.

Recently, weighted gene co-expression network analysis (WGCNA) has been used to construct comprehensive co-expression frameworks from high-dimensional transcriptomes.⁵⁶ We then employed this method to our scRNA-seq data to identify potential co-expressed genes associated with the auxin pathway.

We found 21 genes within a network that showed significant positive or negative correlations using the criteria of absolute value of Pearson correlation coefficient (PCC) > 0.65 and $p < 0.05$ (Figure 5K; Table S11). Two highly co-expressed genes, *Pp3c16_11740* and *Pp3c13_12020* (PCC > 0.99 and $p < 0.001$), encode the enzymes HCT and nucleoside diphosphate kinase 2 (*NDPK2*), whose *Arabidopsis* homologs play roles in auxin transport or response during normal plant growth.^{57,58} Moreover, another gene, *Pp3c2_32400*, encoding a chalcone synthase (*CHS*) whose homologs function as auxin transport inhibitors or competitors of HCT,^{57,59} exhibited negative correlations (absolute PCC > 0.80 and $p < 0.01$) with the *HCT* and *NDPK2* homologs. Interestingly, several carbon fixation- or assimilation-related genes, such as *Pp3c21_14450* and *Pp3c19_1840*, encoding phosphoribulokinase (*PRK*) and Rubisco small subunit 3B (*RBCS3B*), displayed strong positive correlations (PCC > 0.90 and $p < 0.001$) with the *HCT* and *NDPK2* homologs. Notably, the network also detected the two CCM-related genes β CA2 and β CA6. Moreover, 10 transcription factors were found in the co-expression module. For example, the two genes *Pp3c2_4940* and *Pp3c2_31200*, whose *Arabidopsis* homologs *HAT5/HB-1* and *AMS* function as critical regulators for cell development,^{60,61} showed significant positive or negative correlations with the genes involved in auxin transport and CO₂ assimilation (Figure 5K; Table S11). Collectively, these results suggest that carbon fixation/assimilation might be correlated with auxin in *P. patens*.

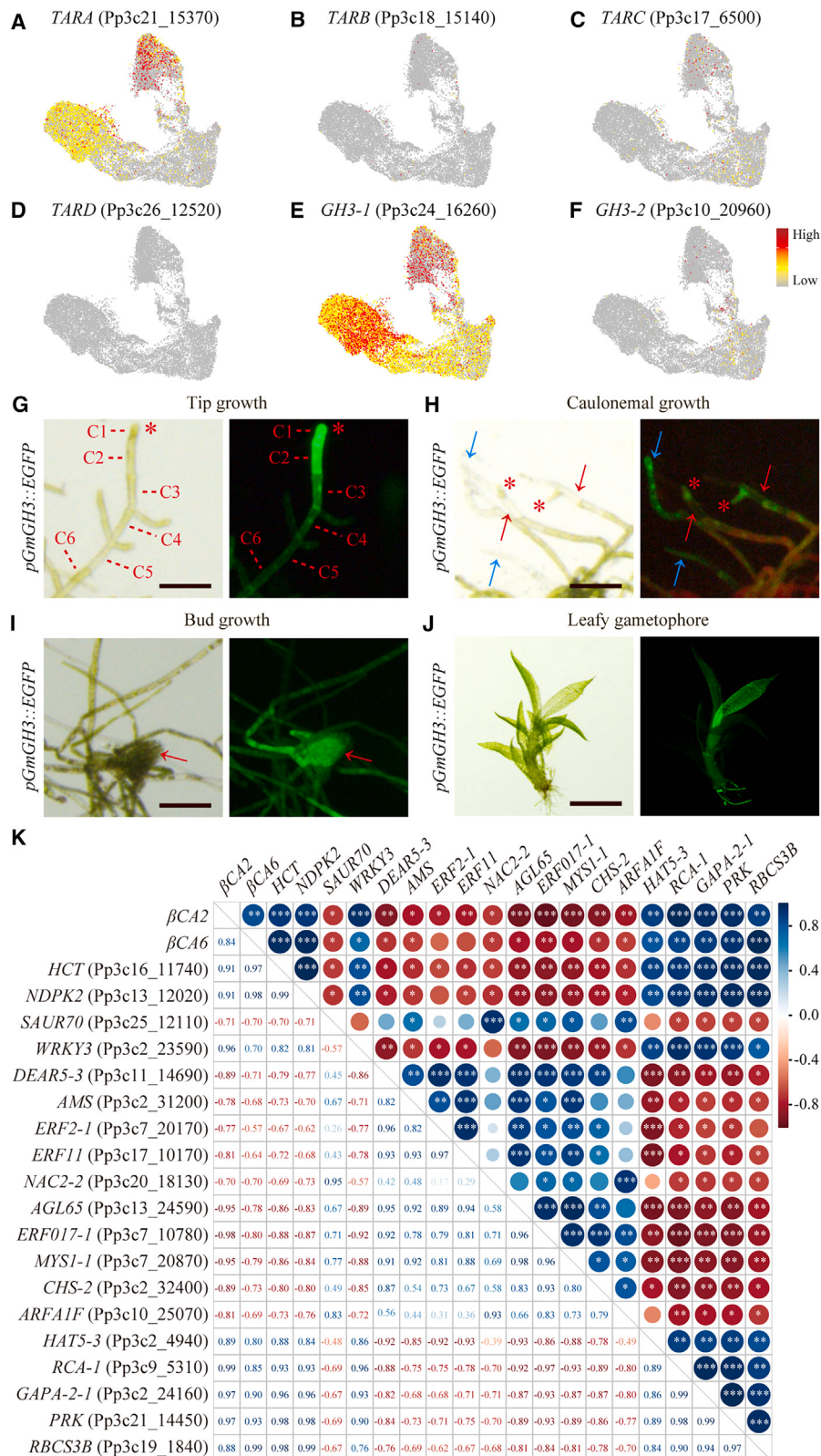
β CAs exhibit distinct cellular expression patterns and play essential roles in 3D gametophore development

Since β CAs might be involved in auxin regulation (Figure 5K), we treated the gametophores of wild-type (WT) plants with 100 μ M L-kynurenone (L-Kyn), an auxin biosynthesis inhibitor, or 0.1% DMSO (solvent control) for 3 weeks (Figures 6A and S16). The plants treated with L-Kyn exhibited severe developmental defects, primarily noticeable at the apex of the gametophores, including irregular leaf elongation and protonema-like cell formation. Intriguingly, six β CAs were all responsive to L-Kyn ($p < 0.05$), particularly β CA2– β CA6, whose relative expression levels showed significant up- or downregulation with more than 2-fold changes (Figure 6B).

Further UMAP visualization demonstrated that these β CAs exhibited distinct cell-type expression patterns (Figures 6C–6H). Similar distributions of low transcript levels were detected between β CA1 and β CA3 (Figures 6C and 6E) and between β CA4 and β CA5 (Figures 6F and 6G). Consistent with the developmental trajectory (Figures 4I and 4K), both β CA2 and β CA6 had relatively high expression levels, resulting in their prominent enrichment in

Figure 4. Trajectories of tip elongation and bud differentiation

- (A) UMAP visualization of clusters 1, 5, and 6.
- (B–E) Expression patterns of genes related to tip growth (*myoXla* and *Rab-E14*) and bud formation (*CLE7* and *RPK2*).^{13,15,18} The color bar denotes relative expression level. Each dot represents a single cell. $n = 5,015$ cells.
- (F) Simulation of the developmental trajectories of tip and bud cells over pseudotime. “Start” indicates the beginning of pseudotime.
- (G–K) Expression patterns of representative genes over the course of tip growth pseudotime.
- (L–P) Expression patterns of representative genes over the course of bud growth pseudotime.
- (Q) Heatmap showing the expression of branch-dependent genes over pseudotime. The branch point represents the start, while both sides indicate the conclusion of pseudotime. Color bar denotes relative expression level. The table on the right shows the symbols of a subset of representative branch-dependent genes. See also Tables S9 and S10.



(legend on next page)

cluster 5 of tip cells (Figures 6D and 6H). Moreover, high levels of β CA2 transcripts were also observed in other cell types, including chloronemal cells (cluster 1), gametophore cells (cluster 3), and bud cells. Likewise, UMAP analysis indicated that numerous transcripts of β CA6 were also expressed in the chloronemal cells (cluster 1). Notably, the cell-type distribution patterns of β CA2 and β CA6 resembled those of their co-expressed genes, including the homologs of *HCT*, *NDPK2*, *HAT5*, and *PRK* (Figures 6D, 6H, and S17). To validate the expression patterns of β CAs *in planta*, we subsequently examined the activities in the following reporter lines: *p β CA2pro:: β CA2-EGFP*, *p β CA3pro:: β CA3-EGFP*, and *p β CA6pro:: β CA6-EGFP* (Figures 6I–6M). Consistent with the scRNA-seq profile, β CA2 activities were highly detected in multiple cell types, including chloronemata, tip-growth cells, and young and mature gametophores (Figures 6I and 6J). By contrast, the β CA3 reporter exhibited predominant activities in dividing chloronemal cells and their side-branch cells (Figure 6K). In agreement with the UMAP analysis, β CA6 was highly expressed during chloronemal outgrowth, particularly in apical and subapical cells along the axis, dividing chloronemal cells, and their side-branch cells (Figure 6L). Interestingly, strong activities of β CA2 and β CA6 were observed at the gametophore apex and in leaf axil cells (Figures 6J and 6M). These findings confirm that β CAs possess diverse cellular expression patterns, potentially playing roles across various cell development processes.

Our previous study revealed that β CAs exhibit functional redundancy, resulting in almost no phenotypic differences between any β ca single mutants and WT plants under normal growth conditions.³⁸ To further explore their roles, we used the CRISPR-LbCas12a gene editing system⁶² to generate multiplex mutants of β CAs. Six guided RNAs were randomly inserted into the CRISPR RNA (crRNA) expression cassette (Figure S18A) and used for subsequent transformation. This strategy resulted in high-efficiency editing events, including targets of β CA2– β CA5 (Figures S18B and S18C). We obtained several types of multiplex mutants as follows: double mutants (β ca2 β ca3, β ca2 β ca4, and β ca3 β ca4), triple mutants (β ca2 β ca3 β ca4), and quadruple mutants (β ca2 β ca3 β ca4 β ca5, hereafter referred to as β caq) (Figures S18D–S18I). However, all double or triple mutants we obtained grew normally, as the WT plants (Figure S19). Intriguingly, the quadruple mutants (β caq#7, β caq#11, and β caq#17) displayed significant defects during mature gametophore development (Figures 6N and 6O). Similar to the L-Kyn treatment in the WT, the leaf morphology in β caq progressively became irregular, starting from the youngest apex to the middle region, accompanied by the emergence of many bulged cells along the leaf mar-

gins (Figure 6N). Closer examination of the apical leaves revealed that numerous chloronema-like cells were formed at the leaf tips in the β caq plants (Figure 6O). In addition, we introduced the *pGmGH3::EGFP* reporter into β caq#7 and found uneven expression patterns in irregular leaves with particularly strong activity at the bulged cells compared to the WT (Figures 6P and 6Q). Taken together, these results illustrate that β CAs play essential roles in gametophore development by affecting the auxin pathway in *P. patens*.

DISCUSSION

3D body patterning is a pivotal morphological innovation that seems to have occurred during the terrestrialization of land plants.^{2,4} The moss *P. patens*, whose life cycle initiates with 2D filaments that possess the capacity for both self-renewal and differentiation into 3D buds,^{6,12} provides an excellent system to investigate the molecular mechanisms underlying the transition from 2D to 3D growth. Although previous research attempted to dissect the mechanisms governing 2D tip or 3D bud cell development through bulk RNA-seq,²² the microdissection methodology was unable to effectively distinguish between morphologically similar cells undergoing tip and bud initiation. Fortunately, the high-resolution scRNA-seq technologies enable us to dissect cellular heterogeneity and elucidate developmental trajectories in plants.⁶³

In this study, we aimed to uncover cellular heterogeneity, identify marker genes, and separate tip or bud cell groups with scRNA-seq profiles. As a result, we assigned ~18,000 cells to seven clusters and predicted five cell types using the tissue- or cell-specific expressed genes identified in earlier studies.^{22,25} We validated the scRNA-seq results using reporter lines *in planta*, thus creating a cell census of the *P. patens* vegetative stage and reconstructing the bud cell differentiation trajectory. Notably, we identified two sub-populations in chloronemata and gametophores. Combined with GO enrichment analyses, we also uncovered their predominant functionalities. Interestingly, the number of CEGs enriched in distinct cell types seemed to be inversely correlated with cell abundance, which was especially evident in the tip and bud cells, implying diverse activities of transcriptional reprogramming. Consistent with a previous study,²² transcripts of genes related to photosynthesis and cell wall biosynthesis were particularly abundant in tip cells and buds, respectively, reflecting distinct physiological signatures.

It is well known that chloronemal cell growth can be initiated in two ways: through its self-renewal or from caulonemal cell

Figure 5. Role of auxin in cell elongation and differentiation across the 2D-to-3D growth of *P. patens*

(A–F) UMAP visualization of expression patterns of four TAR (*TARA-TARD*) and two GH3 (*GH3-1* and *GH3-2*) genes.

(G–J) Expression of the soybean promoter *GmGH3* across 2D-to-3D growth in *P. patens*.

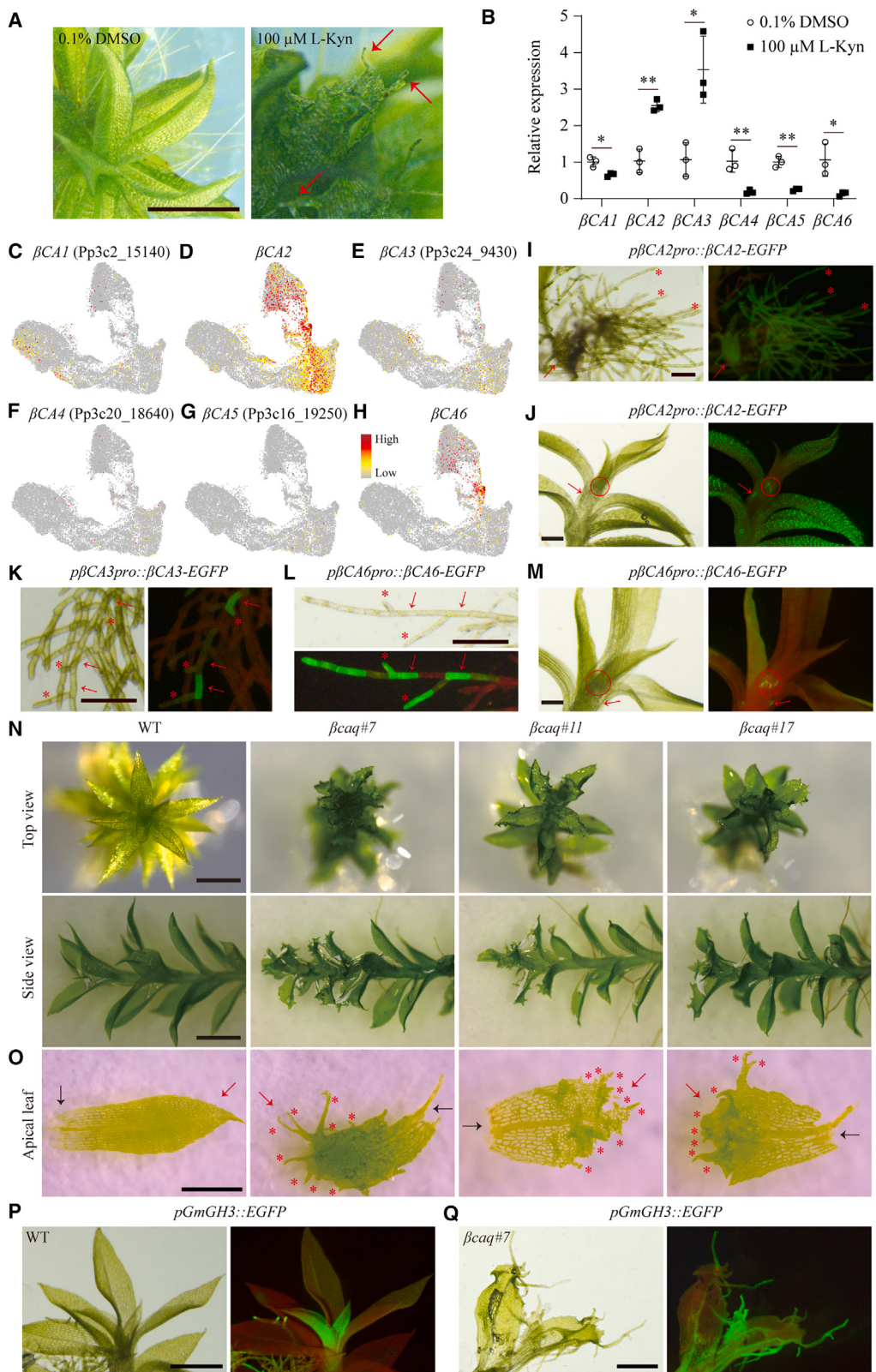
(G) Tip growth (asterisks) in extended chloronemata with side branches. The cells from tip to base along the primary growth direction were labeled as C1–C6. Scale bar: 30 μ m.

(H) Subapical growth (red arrows) in caulonemata displaying side branch initiation (asterisks). Blue arrows denote the caulonemal cells derived from side branch-initiated cells. Scale bar: 30 μ m.

(I) Bud growth (arrows). Scale bar: 30 μ m.

(J) 14-day-old gametophore with leaves and rhizoids. Scale bar: 1 mm.

(K) Co-expression network analysis illuminating the correlation between auxin transport/response and carbon fixation/assimilation. The gene symbols are shown, with blue and red circles representing positive and negative correlations, respectively. Asterisks denote significant correlations among genes with absolute PCC > 0.65 and p < 0.05. * p < 0.05, ** p < 0.01, *** p < 0.001.



(legend on next page)

division.¹⁷ As described previously,¹¹ our observations also suggest that the morphologies of side-branch initial cells closely resembled those of chloronemal cells (Figures 5H, 6K, and 6L). However, the mechanism determining a cell fate of maintaining 2D growth or transitioning to 3D differentiation in newly formed cells remains unclear. By simulating trajectories associated with tip elongation and bud differentiation, we were able to focus on several hundreds of branch-dependent genes. Many auxin-related genes, including homologs of *ALA11*, *AVP1*, *CPI1*, and *SMO1-1*, were highly expressed in cells within the branch of bud differentiation trajectory, which might regulate plant development by affecting auxin production or transport.^{39–41,64} Furthermore, these cells specifically enriched transcripts of genes that might be involved in cell differentiation, such as the homologs of *DGL1* and *PAS2*.^{43,45} By contrast, cells within the tip growth trajectory showed high expression of photosynthesis-related genes, including β CA2 and β CA6. Thus, the molecular signatures that determine strategies between 2D tip elongation and 3D bud transition are significantly distinct.

Previous studies have revealed that auxin signaling is ubiquitous across land plants.^{1,4,48} It has been proposed that, in *P. patens*, the development of 2D filaments and 3D structures, such as tip growth, side branching or bud initiation, gametophore stem elongation, and rhizoid differentiation, likely depends on the auxin activities and their responsiveness.^{11,12,65} This is further supported by the broad yet uneven expression of *TARA* and *GH3-1* in our single-cell atlas. The auxin responsiveness was also verified by the activities of the *GmGH3* promoter in multiple cell types, including chloronema, caulinema, tip-growing cells, side-branch initial cells, bud, gametophore, and rhizoids. However, we were unable to detect the auxin efflux carrier *PIN-FORMED* (*PINA-PINC*) genes that regulate tip growth and gametophore development.^{66,67} This could be due to either the difficulty of capturing cells abundant with their transcripts or their relatively low expression levels in the captured cells.

Although auxin regulation is widespread across the 2D-to-3D growth in *P. patens*, the specific details of the involved molecular machinery remain obscure. For example, what determines the fate of side-branch initial cells, the maintenance of tip growth,

the initiation of buds, and the development of gametophores? Therefore, identifying potential regulators involved in the auxin molecular network is crucial. The application of WGCNA to analyze high-dimensional transcriptomes⁵⁶ enabled us to pinpoint an auxin-relevant co-expression module from the scRNA-seq data. This analysis yielded a network with the homologs of the auxin transport-related genes *HCT* and *NDPK2*.^{57,58} We validated the expression patterns of the co-expressed genes, β CAs, and investigated their roles in leaf cell differentiation by affecting auxin responsiveness during gametophore development. It is well established that β CAs play essential roles in CCM in plants, providing carbon sources (CO_2 or HCO_3^-) for various physiological pathways.⁶⁸ In *Arabidopsis*, β CAs are essential for tapetal cell differentiation,⁶⁹ demonstrating that the partial function of this gene family might be conserved in land plants. However, the multiplex editing of *P. patens* β CAs did not affect the transition from 2D to 3D growth. This could be attributed to their minimal requirements for CCM or the functional redundancy among β CA homologs.³⁸ Additionally, the co-expression of β CAs with a homolog of the transcription factor *HAT5/HB-1*, a known regulator in leaf development,⁶¹ suggests a potential regulatory module.

Collectively, our study represents the application of scRNA-seq to elucidate cellular heterogeneity in a moss. We provided a comprehensive set of molecular markers for various cell types, especially for distinguishing between tip elongation and bud differentiation. Future genetics studies on these identified genes are pivotal to deepen our understanding of the evolutionary mechanisms driving the transition from 2D to 3D growth in land plants.

Limitations of the study

We collected single cells from *P. patens* across 2D to 3D growth to focus on gene expression patterns and heterogeneity. However, the cell census of the rhizoids from the base of the bud/gametophore remains obscure. This might be due to their incomplete specialization with other protonemal cells in the selected samples. Profiling the signatures of rhizoids at single-cell resolution in future studies will help unveil how cells progressively

Figure 6. Significance of β CAs in the development of gametophore leaves in *P. patens*

- (A) The leaf-deficient phenotype observed in WT plants after a treatment with 100 μM L-Kyn compared to those treated with 0.1% DMSO as a control. Red arrows denote the protonema-like cells in the irregular leaves. 14-day-old gametophores were used for treatment. Scale bar: 1.5 mm.
- (B) Expression analysis of six β CAs after L-Kyn treatment. The relative transcript levels in the control were self-normalized to one. Three biological replicates were used, and the values are represented as means \pm SD. Student's t test, * $p < 0.05$, ** $p < 0.01$.
- (C-H) UMAP visualization of β CA expression patterns.
- (I) Expression of *p β CA2pro:: β CA2-EGFP* in protonemata and a young gametophore. Arrows and asterisks denote the gametophore and protonemal tip cells, respectively. Scale bar: 30 μm .
- (J) Expression of *p β CA2pro:: β CA2-EGFP* in a mature gametophore. Circles and arrows denote the apex and leaf axil cells of the gametophore, respectively. Scale bar: 60 μm .
- (K) Expression of *p β CA3pro:: β CA3-EGFP* in chloronemata. Arrows and asterisks denote the dividing chloronemal cells and their side branch cells, respectively. Scale bar: 30 μm .
- (L) Expression of *p β CA6pro:: β CA6-EGFP* in chloronemal tip-growing cells. Arrows and asterisks denote the dividing chloronemal cells and their side branch cells, respectively. Scale bar: 30 μm .
- (M) Expression of *p β CA6pro:: β CA6-EGFP* in a mature gametophore. Circles and arrows denote the apex and leaf axil cells of the gametophore, respectively. Scale bar: 60 μm .
- (N) Developmental defects observed in leaves at the apex of 28-day-old gametophores of *β caq*. Scale bars: 0.5 mm.
- (O) Close-up images of leaves from WT and *β caq* plants. Red and black arrows denote the tip and base of leaves, respectively. Asterisks indicate the chloronema-like cells formed in *β caq* leaves. Scale bar: 0.2 mm.
- (P and Q) Expression of *pGmGH3::EGFP* in apical leaves of WT and *β caq#7* gametophores, respectively. 28-day-old plants were used. Scale bars: 0.5 mm.

differentiate into distinct cell types and increase our understanding of 3D patterning. We also note that many of our observations were based on consistencies with literature and additional experiments. Therefore, further follow-up studies will aid in validating many of our findings, particularly the dynamic expression patterns of marker genes during cell differentiation.

STAR METHODS

Detailed methods are provided in the online version of this paper and include the following:

- KEY RESOURCES TABLE
- RESOURCE AVAILABILITY
 - Lead contact
 - Materials availability
 - Data and code availability
- EXPERIMENTAL MODEL AND STUDY PARTICIPANT DETAILS
 - Plant material and growth conditions
- METHOD DETAILS
 - Protoplast preparation
 - scRNA-seq library construction and sequencing
 - Pre-processing of raw scRNA-seq data
 - Cell clustering by nonlinear dimensional reduction
 - Pseudotime analysis
 - Plasmid construction
 - PEG-mediated transformation
 - Real-time quantitative PCR
 - Microscopy
- QUANTIFICATION AND STATISTICAL ANALYSIS

SUPPLEMENTAL INFORMATION

Supplemental information can be found online at <https://doi.org/10.1016/j.cellrep.2024.114524>.

ACKNOWLEDGMENTS

We thank Dr. Mitsuyasu Hasebe for providing *P. patens* plants and plasmids. We also thank all other members of the Liu lab for helpful discussions regarding the project. This work was supported by the National Natural Science Foundation of China (31971410) and the National Key Research and Development Program of China (2022YFD1200300). The graphical abstract was created with BioRender.

AUTHOR CONTRIBUTIONS

L.L. conceived and supervised the work. Z.C., W.W., and S.Z. performed most experiments and analyzed data. L.L. and Z.C. wrote and revised the paper. L.D. and Z.X. performed some of the experiments and analyses. X.S. and H.H. assisted with writing and interpreted results. All authors read and approved the final manuscript.

DECLARATION OF INTERESTS

The authors declare no competing interests.

Received: November 7, 2023

Revised: May 9, 2024

Accepted: July 8, 2024

Published: July 23, 2024

REFERENCES

1. Bowman, J.L., Kohchi, T., Yamato, K.T., Jenkins, J., Shu, S., Ishizaki, K., Yamaoka, S., Nishihama, R., Nakamura, Y., Berger, F., et al. (2017). Insights into land plant evolution garnered from the *Marchantia polymorpha* genome. *Cell* 171, 287–304.e15. <https://doi.org/10.1016/j.cell.2017.09.030>.
2. Moody, L.A. (2019). The 2D to 3D growth transition in the moss *Physcomitrella patens*. *Curr. Opin. Plant Biol.* 47, 88–95. <https://doi.org/10.1016/j.pbi.2018.10.001>.
3. Rensing, S.A. (2020). How plants conquered land. *Cell* 181, 964–966. <https://doi.org/10.1016/j.cell.2020.05.011>.
4. Zhang, J., Fu, X.X., Li, R.Q., Zhao, X., Liu, Y., Li, M.H., Zwaenepoel, A., Ma, H., Goffinet, B., Guan, Y.L., et al. (2020). The hornwort genome and early land plant evolution. *Nat. Plants* 6, 107–118. <https://doi.org/10.1038/s41477-019-0588-4>.
5. Rensing, S.A., Lang, D., Zimmer, A.D., Terry, A., Salamov, A., Shapiro, H., Nishiyama, T., Perroud, P.F., Lindquist, E.A., Kamisugi, Y., et al. (2008). The *Physcomitrella* genome reveals evolutionary insights into the conquest of land by plants. *Science* 319, 64–69. <https://doi.org/10.1126/science.1150646>.
6. Harrison, C.J., Roeder, A.H., Meyerowitz, E.M., and Langdale, J.A. (2009). Local cues and asymmetric cell divisions underpin body plan transitions in the moss *Physcomitrella patens*. *Curr. Biol.* 19, 461–471. <https://doi.org/10.1016/j.cub.2009.02.050>.
7. Rensing, S.A., Goffinet, B., Meyberg, R., Wu, S.Z., and Bezanilla, M. (2020). The moss *Physcomitrium (Physcomitrella) patens*: a model organism for non-seed plants. *Plant Cell* 32, 1361–1376. <https://doi.org/10.1105/tpc.19.00828>.
8. Cove, D.J., and Knight, C.D. (1993). The moss *Physcomitrella patens*, a model system with potential for the study of plant reproduction. *Plant Cell* 5, 1483–1488. <https://doi.org/10.1105/tpc.5.10.1483>.
9. Menand, B., Calder, G., and Dolan, L. (2007). Both chloronemal and cau-ionemal cells expand by tip growth in the moss *Physcomitrella patens*. *J. Exp. Bot.* 58, 1843–1849. <https://doi.org/10.1093/jxb/erm047>.
10. Kofuji, R., and Hasebe, M. (2014). Eight types of stem cells in the life cycle of the moss *Physcomitrella patens*. *Curr. Opin. Plant Biol.* 17, 13–21. <https://doi.org/10.1016/j.pbi.2013.10.007>.
11. Thelander, M., Landberg, K., and Sundberg, E. (2018). Auxin-mediated developmental control in the moss *Physcomitrella patens*. *J. Exp. Bot.* 69, 277–290. <https://doi.org/10.1093/jxb/erx255>.
12. Aoyama, T., Hiwatashi, Y., Shigyo, M., Kofuji, R., Kubo, M., Ito, M., and Hasebe, M. (2012). AP2-type transcription factors determine stem cell identity in the moss *Physcomitrella patens*. *Development* 139, 3120–3129. <https://doi.org/10.1242/dev.076091>.
13. Vidali, L., Burkart, G.M., Augustine, R.C., Kerndavid, E., Tüzel, E., and Bezanilla, M. (2010). Myosin XI is essential for tip growth in *Physcomitrella patens*. *Plant Cell* 22, 1868–1882. <https://doi.org/10.1105/tpc.109.073288>.
14. Yi, P., and Goshima, G. (2020). Rho of plants GTPases and cytoskeletal elements control nuclear positioning and asymmetric cell division during *Physcomitrella patens* branching. *Curr. Biol.* 30, 2860–2868.e3. <https://doi.org/10.1016/j.cub.2020.05.022>.
15. Orr, R.G., Furt, F., Warner, E.L., Agar, E.M., Garbarino, J.M., Cabral, S.E., Dubuke, M.L., Butt, A.M., Munson, M., and Vidali, L. (2021). Rab-E and its interaction with myosin XI are essential for polarised cell growth. *New Phytol.* 229, 1924–1936. <https://doi.org/10.1111/nph.17023>.
16. Perroud, P.F., Demko, V., Johansen, W., Wilson, R.C., Olsen, O.A., and Quatrano, R.S. (2014). Defective Kernel 1 (DEK1) is required for three-dimensional growth in *Physcomitrella patens*. *New Phytol.* 203, 794–804. <https://doi.org/10.1111/nph.12844>.
17. Moody, L.A., Kelly, S., Rabbinowitsch, E., and Langdale, J.A. (2018). Genetic regulation of the 2D to 3D growth transition in the moss *Physcomitrella patens*. *Curr. Biol.* 28, 473–478.e5. <https://doi.org/10.1016/j.cub.2017.12.052>.
18. Whitewoods, C.D., Cammarata, J., Nemec Venza, Z., Sang, S., Crook, A.D., Aoyama, T., Wang, X.Y., Waller, M., Kamisugi, Y., Cuming, A.C.,

- et al. (2018). CLAVATA was a genetic novelty for the morphological innovation of 3D growth in land plants. *Curr. Biol.* 28, 2365–2376.e5. <https://doi.org/10.1016/j.cub.2018.05.068>.
19. Moody, L.A., Kelly, S., Clayton, R., Weeks, Z., Emms, D.M., and Langdale, J.A. (2021). NO GAMETOPHORES 2 is a novel regulator of the 2D to 3D growth transition in the moss *Physcomitrella patens*. *Curr. Biol.* 31, 555–563.e4. <https://doi.org/10.1016/j.cub.2020.10.077>.
 20. Nemec-Venza, Z., Madden, C., Stewart, A., Liu, W., Novák, O., Pěnčík, A., Cuming, A.C., Kamisugi, Y., and Harrison, C.J. (2022). CLAVATA modulates auxin homeostasis and transport to regulate stem cell identity and plant shape in a moss. *New Phytol.* 234, 149–163. <https://doi.org/10.1111/nph.17969>.
 21. Kriegshauser, L., Knosp, S., Grienberger, E., Tatsumi, K., Gütle, D.D., Sørensen, I., Herrgott, L., Zumsteg, J., Rose, J.K.C., Reski, R., et al. (2021). Function of the HYDROXYCINNAMOYL-CoA:SHIKIMATE HYDROXYCINNAMOYL TRANSFERASE is evolutionarily conserved in embryophytes. *Plant Cell* 33, 1472–1491. <https://doi.org/10.1093/plcell/koab044>.
 22. Frank, M.H., and Scanlon, M.J. (2015). Cell-specific transcriptomic analyses of three-dimensional shoot development in the moss *Physcomitrella patens*. *Plant J.* 83, 743–751. <https://doi.org/10.1111/tpj.12928>.
 23. Chen, H., Yin, X., Guo, L., Yao, J., Ding, Y., Xu, X., Liu, L., Zhu, Q.H., Chu, Q., and Fan, L. (2021). PlantscRNADB: a database for plant single-cell RNA analysis. *Mol. Plant* 14, 855–857. <https://doi.org/10.1016/j.molp.2021.05.002>.
 24. Jin, J., Lu, P., Xu, Y., Tao, J., Li, Z., Wang, S., Yu, S., Wang, C., Xie, X., Gao, J., et al. (2022). PCMDB: a curated and comprehensive resource of plant cell markers. *Nucleic Acids Res.* 50, D1448–D1455. <https://doi.org/10.1093/nar/gkab949>.
 25. Ortiz-Ramírez, C., Hernandez-Coronado, M., Thamm, A., Catarino, B., Wang, M., Dolan, L., Feijó, J.A., and Becker, J.D. (2016). A transcriptome atlas of *Physcomitrella patens* provides insights into the evolution and development of land plants. *Mol. Plant* 9, 205–220. <https://doi.org/10.1016/j.molp.2015.12.002>.
 26. Vidali, L., and Bezanilla, M. (2012). *Physcomitrella patens*: a model for tip cell growth and differentiation. *Curr. Opin. Plant Biol.* 15, 625–631. <https://doi.org/10.1016/j.pbi.2012.09.008>.
 27. Jones, M.A., Covington, M.F., DiTacchio, L., Vollmers, C., Panda, S., and Harmer, S.L. (2010). Jumonji domain protein JMJD5 functions in both the plant and human circadian systems. *Proc. Natl. Acad. Sci. USA* 107, 21623–21628. <https://doi.org/10.1073/pnas.1014204108>.
 28. Liu, Z., Jia, Y., Ding, Y., Shi, Y., Li, Z., Guo, Y., Gong, Z., and Yang, S. (2017). Plasma membrane CRPK1-mediated phosphorylation of 14-3-3 proteins induces their nuclear import to fine-tune CBF signaling during cold response. *Mol. Cell* 66, 117–128.e5. <https://doi.org/10.1016/j.molcel.2017.02.016>.
 29. Abrieux, A., Xue, Y., Cai, Y., Lewald, K.M., Nguyen, H.N., Zhang, Y., and Chiu, J.C. (2020). EYES ABSENT and TIMELESS integrate photoperiodic and temperature cues to regulate seasonal physiology in *Drosophila*. *Proc. Natl. Acad. Sci. USA* 117, 15293–15304. <https://doi.org/10.1073/pnas.2004262117>.
 30. Fujii, H., and Zhu, J.K. (2009). *Arabidopsis* mutant deficient in 3 abscisic acid-activated protein kinases reveals critical roles in growth, reproduction, and stress. *Proc. Natl. Acad. Sci. USA* 106, 8380–8385. <https://doi.org/10.1073/pnas.0903144106>.
 31. Ahn, S.J., Shin, R., and Schachtman, D.P. (2004). Expression of KT/KUP genes in *Arabidopsis* and the role of root hairs in K⁺ uptake. *Plant Physiol.* 134, 1135–1145. <https://doi.org/10.1104/pp.103.034660>.
 32. Versaw, W.K., and Harrison, M.J. (2002). A chloroplast phosphate transporter, PHT2;1, influences allocation of phosphate within the plant and phosphate-starvation responses. *Plant Cell* 14, 1751–1766. <https://doi.org/10.1105/tpc.002220>.
 33. El Houari, I., Van Beirs, C., Arents, H.E., Han, H., Chanoca, A., Opdenacker, D., Pollier, J., Storme, V., Steenackers, W., Quareshy, M., et al. (2021). Seedling developmental defects upon blocking CINNAMATE-4-HYDROXYLASE are caused by perturbations in auxin transport. *New Phytol.* 230, 2275–2291. <https://doi.org/10.1111/nph.17349>.
 34. Strader, L.C., Wheeler, D.L., Christensen, S.E., Berens, J.C., Cohen, J.D., Rampey, R.A., and Bartel, B. (2011). Multiple facets of *Arabidopsis* seedling development require indole-3-butryric acid-derived auxin. *Plant Cell* 23, 984–999. <https://doi.org/10.1105/tpc.111.083071>.
 35. Ishikawa, M., Murata, T., Sato, Y., Nishiyama, T., Hiwatashi, Y., Imai, A., Kimura, M., Sugimoto, N., Akita, A., Oguri, Y., et al. (2011). *Physcomitrella* cyclin-dependent kinase A links cell cycle reactivation to other cellular changes during reprogramming of leaf cells. *Plant Cell* 23, 2924–2938. <https://doi.org/10.1105/tpc.111.088005>.
 36. Trapnell, C., Cacchiarelli, D., Grimsby, J., Pokharel, P., Li, S., Morse, M., Lennon, N.J., Livak, K.J., Mikkelsen, T.S., and Rinn, J.L. (2014). The dynamics and regulators of cell fate decisions are revealed by pseudotemporal ordering of single cells. *Nat. Biotechnol.* 32, 381–386. <https://doi.org/10.1038/nbt.2859>.
 37. Qiu, X., Hill, A., Packer, J., Lin, D., Ma, Y.A., and Trapnell, C. (2017). Single-cell mRNA quantification and differential analysis with Census. *Nat. Methods* 14, 309–315. <https://doi.org/10.1038/nmeth.4150>.
 38. Chen, Z., Wang, W., Dong, X., Pu, X., Gao, B., and Liu, L. (2020). Functional redundancy and divergence of β-carbonic anhydrases in *Physcomitrella patens*. *Planta* 252, 20. <https://doi.org/10.1007/s00425-020-03429-8>.
 39. Li, J., Yang, H., Peer, W.A., Richter, G., Blakeslee, J., Bandyopadhyay, A., Titapiwantakun, B., Undurraga, S., Khodakovskaya, M., Richards, E.L., et al. (2005). *Arabidopsis* H⁺-PPase AVP1 regulates auxin-mediated organ development. *Science* 310, 121–125. <https://doi.org/10.1126/science.1115711>.
 40. Men, S., Boutté, Y., Ikeda, Y., Li, X., Palme, K., Stierhof, Y.D., Hartmann, M.A., Moritz, T., and Grebe, M. (2008). Sterol-dependent endocytosis mediates post-cytokinetic acquisition of PIN2 auxin efflux carrier polarity. *Nat. Cell Biol.* 10, 237–244. <https://doi.org/10.1038/ncb1686>.
 41. Zhang, X., Adamowski, M., Marhava, P., Tan, S., Zhang, Y., Rodriguez, L., Zwiewka, M., Pukyšová, V., Sánchez, A.S., Raxwal, V.K., et al. (2020). *Arabidopsis* flippases cooperate with ARF GTPase exchange factors to regulate the trafficking and polarity of PIN auxin transporters. *Plant Cell* 32, 1644–1664. <https://doi.org/10.1105/tpc.19.00869>.
 42. Li, L., Verstraeten, I., Roosjen, M., Takahashi, K., Rodriguez, L., Merrin, J., Chen, J., Shabala, L., Smet, W., Ren, H., et al. (2021). Cell surface and intracellular auxin signalling for H⁺ fluxes in root growth. *Nature* 599, 273–277. <https://doi.org/10.1038/s41586-021-04037-6>.
 43. Lerouxel, O., Mouille, G., Andème-Onzighi, C., Bruyant, M.P., Séveno, M., Loutelier-Bourhis, C., Driouich, A., Höfte, H., and Lerouge, P. (2005). Mutants in DEFECTIVE GLYCOSYLATION, an *Arabidopsis* homolog of an oligosaccharyltransferase complex subunit, show protein underglycosylation and defects in cell differentiation and growth. *Plant J.* 42, 455–468. <https://doi.org/10.1111/j.1365-313X.2005.02392.x>.
 44. Chen, M., Han, G., Dietrich, C.R., Dunn, T.M., and Cahoon, E.B. (2006). The essential nature of sphingolipids in plants as revealed by the functional identification and characterization of the *Arabidopsis* LCB1 subunit of serine palmitoyltransferase. *Plant Cell* 18, 3576–3593. <https://doi.org/10.1105/tpc.105.040774>.
 45. Da Costa, M., Bach, L., Landrieu, I., Belloc, Y., Catrice, O., Brown, S., De Veylder, L., Lippens, G., Inzé, D., and Faure, J.D. (2006). *Arabidopsis* PASTICCINO2 is an antiphosphatase involved in regulation of cyclin-dependent kinase A. *Plant Cell* 18, 1426–1437. <https://doi.org/10.1105/tpc.105.040485>.
 46. Ishiguro, S., Watanabe, Y., Ito, N., Nonaka, H., Takeda, N., Sakai, T., Kanaya, H., and Okada, K. (2002). SHEPHERD is the *Arabidopsis* GRP94

- responsible for the formation of functional CLAVATA proteins. *EMBO J.* 21, 898–908. <https://doi.org/10.1093/emboj/21.5.898>.
47. Mano, Y., and Nemoto, K. (2012). The pathway of auxin biosynthesis in plants. *J. Exp. Bot.* 63, 2853–2872. <https://doi.org/10.1093/jxb/ers091>.
 48. Thelander, M., Landberg, K., Muller, A., Cloarec, G., Cunniffe, N., Huguet, S., Soubigou-Taconnat, L., Brunaud, V., and Couder, Y. (2022). Apical dominance control by *TAR-YUC*-mediated auxin biosynthesis is a deep homology of land plants. *Curr. Biol.* 32, 3838–3846.e5. <https://doi.org/10.1016/j.cub.2022.06.064>.
 49. Hagen, G., Kleinschmidt, A., and Guilfoyle, T. (1984). Auxin-regulated gene expression in intact soybean hypocotyl and excised hypocotyl sections. *Planta* 162, 147–153. <https://doi.org/10.1007/BF00410211>.
 50. Hagen, G., and Guilfoyle, T.J. (1985). Rapid induction of selective transcription by auxins. *Mol. Cell Biol.* 5, 1197–1203. <https://doi.org/10.1128/mcb.5.6.1197-1203.1985>.
 51. Staswick, P.E., Serban, B., Rowe, M., Tiryaki, I., Maldonado, M.T., Maldonado, M.C., and Suza, W. (2005). Characterization of an *Arabidopsis* enzyme family that conjugates amino acids to indole-3-acetic acid. *Plant Cell* 17, 616–627. <https://doi.org/10.1105/tpc.104.026690>.
 52. Ludwig-Müller, J., Jülke, S., Bierfreund, N.M., Decker, E.L., and Reski, R. (2009). Moss (*Physcomitrella patens*) GH3 proteins act in auxin homeostasis. *New Phytol.* 181, 323–338. <https://doi.org/10.1111/j.1469-8137.2008.02677.x>.
 53. Böttcher, C., Keyzers, R.A., Boss, P.K., and Davies, C. (2010). Sequestration of auxin by the indole-3-acetic acid-amido synthetase GH3-1 in grape berry (*Vitis vinifera* L.) and the proposed role of auxin conjugation during ripening. *J. Exp. Bot.* 61, 3615–3625. <https://doi.org/10.1093/jxb/erq174>.
 54. Bierfreund, N.M., Reski, R., and Decker, E.L. (2003). Use of an inducible reporter gene system for the analysis of auxin distribution in the moss *Physcomitrella patens*. *Plant Cell Rep.* 21, 1143–1152. <https://doi.org/10.1007/s00299-003-0646-1>.
 55. Thelander, M., Landberg, K., and Sundberg, E. (2019). Minimal auxin sensing levels in vegetative moss stem cells revealed by a ratiometric reporter. *New Phytol.* 224, 775–788. <https://doi.org/10.1111/nph.16068>.
 56. Morabito, S., Reese, F., Rahimzadeh, N., Miyoshi, E., and Swarup, V. (2023). hdWGCA identifies co-expression networks in high-dimensional transcriptomics data. *Cell Rep. Methods* 3, 100498. <https://doi.org/10.1016/j.crmeth.2023.100498>.
 57. Besseau, S., Hoffmann, L., Geoffroy, P., Lapierre, C., Pollet, B., and Le-grand, M. (2007). Flavonoid accumulation in *Arabidopsis* repressed in lignin synthesis affects auxin transport and plant growth. *Plant Cell* 19, 148–162. <https://doi.org/10.1105/tpc.106.044495>.
 58. Choi, G., Kim, J.I., Hong, S.W., Shin, B., Choi, G., Blakeslee, J.J., Murphy, A.S., Seo, Y.W., Kim, K., Koh, E.J., et al. (2005). A possible role for NDPK2 in the regulation of auxin-mediated responses for plant growth and development. *Plant Cell Physiol.* 46, 1246–1254. <https://doi.org/10.1093/pcp/pci133>.
 59. Wasson, A.P., Pellerone, F.I., and Mathesius, U. (2006). Silencing the flavonoid pathway in *Medicago truncatula* inhibits root nodule formation and prevents auxin transport regulation by rhizobia. *Plant Cell* 18, 1617–1629. <https://doi.org/10.1105/tpc.105.038232>.
 60. Xu, J., Yang, C., Yuan, Z., Zhang, D., Gondwe, M.Y., Ding, Z., Liang, W., Zhang, D., and Wilson, Z.A. (2010). The ABORTED MICROSPORES regulatory network is required for postmeiotic male reproductive development in *Arabidopsis thaliana*. *Plant Cell* 22, 91–107. <https://doi.org/10.1105/tpc.109.071803>.
 61. Miguel, V.N., Manavella, P.A., Chan, R.L., and Capella, M.A. (2020). The AtHB1 transcription factor controls the miR164-CUC2 regulatory node to modulate leaf development. *Plant Cell Physiol.* 61, 659–670. <https://doi.org/10.1093/pcp/pcz233>.
 62. Pu, X., Liu, L., Li, P., Huo, H., Dong, X., Xie, K., Yang, H., and Liu, L. (2019). A CRISPR/LbCas12a-based method for highly efficient multiplex gene ed-
 - iting in *Physcomitrella patens*. *Plant J.* 100, 863–872. <https://doi.org/10.1111/tpj.14478>.
 63. Seyfferth, C., Renema, J., Wendrich, J.R., Eekhout, T., Seurinck, R., Vandamme, N., Blob, B., Saeys, Y., Helariutta, Y., Birnbaum, K.D., and De Rybel, B. (2021). Advances and opportunities in single-cell transcriptomics for plant research. *Annu. Rev. Plant Biol.* 72, 847–866. <https://doi.org/10.1146/annurev-aplant-081720-010120>.
 64. Song, J., Sun, S., Ren, H., Grison, M., Boutté, Y., Bai, W., and Men, S. (2019). The SMO1 family of sterol 4 α -methyl oxidases is essential for auxin- and cytokinin-regulated embryogenesis. *Plant Physiol.* 181, 578–594. <https://doi.org/10.1104/pp.19.00144>.
 65. Lavy, M., Prigge, M.J., Tao, S., Shain, S., Kuo, A., Kirchsteiger, K., and Estelle, M. (2016). Constitutive auxin response in *Physcomitrella* reveals complex interactions between Aux/IAA and ARF proteins. *Elife* 5, e13325. <https://doi.org/10.7554/elife.13325>.
 66. Bennett, T.A., Liu, M.M., Aoyama, T., Bierfreund, N.M., Braun, M., Couder, Y., Dennis, R.J., O'Connor, D., Wang, X.Y., White, C.D., et al. (2014). Plasma membrane-targeted PIN proteins drive shoot development in a moss. *Curr. Biol.* 24, 2776–2785. <https://doi.org/10.1016/j.cub.2014.09.054>.
 67. Viaene, T., Landberg, K., Thelander, M., Medvecka, E., Pederson, E., Feraru, E., Cooper, E.D., Karimi, M., Delwiche, C.F., Ljung, K., et al. (2014). Directional auxin transport mechanisms in early diverging land plants. *Curr. Biol.* 24, 2786–2791. <https://doi.org/10.1016/j.cub.2014.09.056>.
 68. DiMario, R.J., Clayton, H., Mukherjee, A., Ludwig, M., and Moroney, J.V. (2017). Plant carbonic anhydrases: structures, locations, evolution, and physiological roles. *Mol. Plant* 10, 30–46. <https://doi.org/10.1016/j.molp.2016.09.001>.
 69. Huang, J., Li, Z., Biener, G., Xiong, E., Malik, S., Eaton, N., Zhao, C.Z., Raicu, V., Kong, H., and Zhao, D. (2017). Carbonic anhydrases function in anther cell differentiation downstream of the receptor-like kinase EMS1. *Plant Cell* 29, 1335–1356. <https://doi.org/10.1105/tpc.16.00484>.
 70. Wu, T., Hu, E., Xu, S., Chen, M., Guo, P., Dai, Z., Feng, T., Zhou, L., Tang, W., Zhan, L., et al. (2021). clusterProfiler 4.0: a universal enrichment tool for interpreting omics data. *Innovation* 2, 100141. <https://doi.org/10.1016/j.inn.2021.100141>.
 71. Huerta-Cepas, J., Szklarczyk, D., Heller, D., Hernández-Plaza, A., Forsslund, S.K., Cook, H., Mende, D.R., Letunic, I., Rattei, T., Jensen, L.J., et al. (2019). eggNOG 5.0: a hierarchical, functionally and phylogenetically annotated orthology resource based on 5090 organisms and 2502 viruses. *Nucleic Acids Res.* 47, D309–D314. <https://doi.org/10.1093/nar/gky1085>.
 72. Hao, Y., Hao, S., Andersen-Nissen, E., Mauck, W.M., 3rd, Zheng, S., Butler, A., Lee, M.J., Wilk, A.J., Darby, C., Zager, M., et al. (2021). Integrated analysis of multimodal single-cell data. *Cell* 184, 3573–3587.e29. <https://doi.org/10.1016/j.cell.2021.04.048>.
 73. Liu, H., Ding, Y., Zhou, Y., Jin, W., Xie, K., and Chen, L.L. (2017). CRISPR-P 2.0: an improved CRISPR-Cas9 tool for genome editing in plants. *Mol. Plant* 10, 530–532. <https://doi.org/10.1016/j.molp.2017.01.003>.
 74. Ding, J., Adiconis, X., Simmons, S.K., Kowalczyk, M.S., Hession, C.C., Marjanovic, N.D., Hughes, T.K., Wadsworth, M.H., Burks, T., Nguyen, L.T., et al. (2020). Systematic comparison of single-cell and single-nucleus RNA-sequencing methods. *Nat. Biotechnol.* 38, 737–746. <https://doi.org/10.1038/s41587-020-0465-8>.
 75. Becht, E., McInnes, L., Healy, J., Dutertre, C.A., Kwok, I.W.H., Ng, L.G., Ginhoux, F., and Newell, E.W. (2018). Dimensionality reduction for visualizing single-cell data using t-SNE. *Nat. Biotechnol.* 37, 38–44. <https://doi.org/10.1038/nbt.4314>.
 76. Kobak, D., and Berens, P. (2019). The art of using t-SNE for single-cell transcriptomics. *Nat. Commun.* 10, 5416. <https://doi.org/10.1038/s41467-019-13056-x>.

77. Zhang, T.Q., Chen, Y., and Wang, J.W. (2021). A single-cell analysis of the *Arabidopsis* vegetative shoot apex. *Dev. Cell* 56, 1056–1074.e8. <https://doi.org/10.1016/j.devcel.2021.02.021>.
78. Collonnier, C., Epert, A., Mara, K., Maclot, F., Guyon-Debast, A., Charlöt, F., White, C., Schaefer, D.G., and Nogué, F. (2017). CRISPR-Cas9-mediated efficient directed mutagenesis and RAD51-dependent and RAD51-independent gene targeting in the moss *Physcomitrella patens*. *Plant Biotechnol. J.* 15, 122–131. <https://doi.org/10.1111/pbi.12596>.
79. Nishiyama, T., Hiwatashi, Y., Sakakibara, I., Kato, M., and Hasebe, M. (2000). Tagged mutagenesis and gene-trap in the moss, *Physcomitrella patens* by shuttle mutagenesis. *DNA Res.* 7, 9–17. <https://doi.org/10.1093/dnares/7.1.9>.
80. Liu, L., McNeilage, R.T., Shi, L.X., and Theg, S.M. (2014). ATP requirement for chloroplast protein import is set by the K_m for ATP hydrolysis of stromal Hsp70 in *Physcomitrella patens*. *Plant Cell* 26, 1246–1255. <https://doi.org/10.1105/tpc.113.121822>.

STAR★METHODS

KEY RESOURCES TABLE

REAGENT or RESOURCE	SOURCE	IDENTIFIER
Bacterial and virus strains		
<i>Escherichia coli</i> strain DH5a	Weidi	Cat# DL1001
Chemicals, peptides, and recombinant proteins		
L-Kyn	Sigma-Aldrich	K8625; CAS 2922-83-0
DMSO	Sigma-Aldrich	D4540; CAS 67-68-5
G418 Sulfate	Macklin	G6021; CAS 108321-42-2
Hygromycin B	Macklin	H6134; CAS 31282-04-9
Potassium nitrate	Sigma-Aldrich	P8291; CAS 7757-79-1
Calcium nitrate tetrahydrate	Sigma-Aldrich	C2786; CAS 13477-34-4
Tris	Sangon Biotech	A501492; CAS 77-86-1
MES monohydrate	Sangon Biotech	A610341; CAS 145224-94-8
Magnesium chloride hexahydrate	Sangon Biotech	A601336; CAS 7791-18-6
Ammonium tartrate dibasic	Sigma-Aldrich	09985; CAS 3164-29-2
Calcium chloride dihydrate	Sigma-Aldrich	V900269; CAS 10035-04-8
PEG	Sigma-Aldrich	81240; CAS 25322-68-3
D-Mannitol	Sangon Biotech	A600335; CAS 69-65-8
Driselase	Sigma-Aldrich	D8037; CAS 85186-71-6
Critical commercial assays		
Chromium Next GEM Single Cell 3' Kit v3.1	10x Genomics	Cat# PN-1000269
Plant Total RNA Isolation Kit	Vazyme	Cat# RC411
One Step Cloning Kit	Vazyme	Cat# C112
Uni RT&qPCR Kit	Transgen	Cat# AUQ-01
Deposited data		
Data for scRNA-seq	This study	China National Center for Bioinformation: PRJCA020730
Experimental models: Organisms/strains		
<i>Physcomitrium</i> ecotype Gransden	National Institute for Basic Biology	https://moss.nibb.ac.jp/contact.html
<i>JMJD5pro::EGFP</i>	This study	N/A
<i>CRPK1pro::EGFP</i>	This study	N/A
<i>EYAPro::EGFP</i>	This study	N/A
<i>OST1pro::EGFP</i>	This study	N/A
<i>KUP3pro::EGFP</i>	This study	N/A
<i>PSBO2-1pro::EGFP</i>	This study	N/A
<i>PHT2;1pro::EGFP</i>	This study	N/A
<i>βCA2pro::βCA2-EGFP</i>	This study	N/A
<i>βCA3pro::βCA3-EGFP</i>	This study	N/A
<i>βCA6pro::βCA6-EGFP</i>	This study	N/A
<i>βca2βca3</i>	This study	N/A
<i>βca2βca4</i>	This study	N/A
<i>βca3βca4</i>	This study	N/A
<i>βca2βca3βca4βca5 (βcaq)</i>	This study	N/A
<i>GmGH3::EGFP</i>	This study	N/A
<i>GmGH3::EGFP βcaq</i>	This study	N/A

(Continued on next page)

Continued

REAGENT or RESOURCE	SOURCE	IDENTIFIER
Oligonucleotides		
See Table S12	This study	N/A
Recombinant DNA		
Plasmid: pJMJD5pro:EGFP	This study	N/A
Plasmid: pCRPK1pro:EGFP	This study	N/A
Plasmid: pEYAPro:EGFP	This study	N/A
Plasmid: pOST1pro:EGFP	This study	N/A
Plasmid: pKUP3pro:EGFP	This study	N/A
Plasmid: pPSBO2-1pro:EGFP	This study	N/A
Plasmid: pPHT2; 1pro:EGFP	This study	N/A
Plasmid: pβCA2pro:βCA2-EGFP	This study	N/A
Plasmid: pβCA3pro:βCA3-EGFP	This study	N/A
Plasmid: pβCA6pro:βCA6-EGFP	This study	N/A
Plasmid: pGmGH3:EGFP	This study	N/A
Plasmid: pU6:crRNA-βCAs	This study	N/A
Software and algorithms		
Cellranger (v.3.1.0)	10x Genomics	https://www.10xgenomics.com/support/software/cell-ranger/downloads/previous-versions
clusterProfiler (v4.0)	Wu et al. ⁷⁰	https://github.com/YuLab-SMU/clusterProfiler
EggNOG (v5.0)	Huerta-Cepas et al. ⁷¹	http://eggnog-mapper.embl.de/
Seurat (v4.3.0)	Hao et al. ⁷²	https://github.com/satijalab/seurat
Monocle (v2.26.0)	Trapnell et al. ³⁶ Qiu et al. ³⁷	https://bioconductor.org/packages/release/bioc/html/monocle.html
hdWGCNA (v.0.2.16)	Morabito et al. ⁵⁶	https://smorabit.github.io/hdWGCNA/
CRISPR-P (v2.0)	Liu et al. ⁷³	http://crispr.hzau.edu.cn/cgi-bin/CRISPR2/CRISPR
R software (v4.2.1)	R Foundation	https://www.r-project.org

RESOURCE AVAILABILITY

Lead contact

Further information and requests for resources and reagents should be directed to and will be fulfilled by the lead contact, Li Liu (liuli2020@hubu.edu.cn).

Materials availability

Plasmids and plant materials generated in this research are all available on request to the lead contact, Li Liu (liuli2020@hubu.edu.cn).

Data and code availability

- The raw sequencing data have been deposited at the Genome Sequence Archive (GSA): CRA013145 and are publicly available as of the date of publication. The bioproject ID is listed in the [key resources table](#).
- This paper does not report original code.
- Any additional information required to reanalyze the data reported in this paper is available from the [lead contact](#) upon request.

EXPERIMENTAL MODEL AND STUDY PARTICIPANT DETAILS

Plant material and growth conditions

All wild-type and transgenic lines used here were *Physcomitrium patens* ecotype Gransden. *Physcomitrium* wild-type was obtained from Professor Mitsuyasu Hasebe (National Institute for Basic Biology, Japan) and was used in single-cell RNA sequencing. The sporangia were surface sterilized in 10% sodium hypochlorite for 5 min, followed by washing with sterilized water 10 times. Subsequently, each sporangium was crushed by the tip of a blue pipetman and the dispersed spores were poured onto the cellophane-overlaid BCDAT medium. The spores were continuously incubated for one or two weeks to produce protonemata and gametophores under a long photoperiod (16L/8D) at 25°C. For pharmacological treatment, 100 mM stock solutions of L-Kyn (Sigma-Aldrich) were

prepared in DMSO (Sigma-Aldrich). Gametophores were treated with either 100 μ M L-Kyn or 0.1% DMSO (a solvent control) for three weeks and used for microscopy analyses.

METHOD DETAILS

Protoplast preparation

Plants were repeatedly propagated on cellophane-overlaid petri dishes to produce homogeneous protonemata, which were then cultured for an additional 14 days to initiate bud formation and to grow young gametophores. The cultures were collected and digested with 30 mL of 2% (w/v) Driselase (Sigma-Aldrich) enzyme solution (prepared in 8% D-Mannitol). After digesting for 45 min, the protoplasts were filtered through a 40 μ m nylon mesh into a round-bottomed tube and centrifuged at 800 rpm for 10 min at 25°C using a swinging rotor. The pelleted protoplasts were gently resuspended in 30 mL of 8% D-Mannitol and centrifuged at 800 rpm for 10 min at 25°C. Intact protoplasts remained pelleted at the bottom. The supernatant was removed and protoplast pellets were suspended in 30 mL of protoplast buffer (0.5 M D-Mannitol, 15 mM Magnesium chloride, and 0.1% MES pH 5.6). The protoplast viability was assessed with a hemocytometer using 0.4% trypan blue solution and diameters were determined by ImageJ. Only those preparations with protoplast viability exceeding 85% were processed with the 10 \times Genomics Single Cell Protocol (CG00052, RevC), and triplicates were applied to these samples.

scRNA-seq library construction and sequencing

Library preparations for scRNA-seq were performed as previously described.⁷⁴ The final concentration of protoplast was diluted to 1,000 cells/ μ L. Approximately 7,000 cells were loaded into each channel from the Chromium Next GEM Single Cell 3' Kit v3.1 (10 \times Genomics). Protoplasts were barcoded with a Chromium Chip (10 \times Genomics) in 10 \times Chip Holder to generate single-cell GEM (Gel Bead in emulsion) for library construction. 65 μ L of PCR Amplification Mix was added to each sample, and mRNA reverse transcription was performed on a thermal cycler as follows: 98°C for 3 min, 11 cycles of 98°C for 15 s, 63°C for 20 s, and 72°C for 1 min, followed by a final extension at 72°C for 1 min, and cooled to 4°C. The final quality of the cDNA libraries was assessed using a Bio-analyzer 2100 (Agilent). The resulting cDNA libraries were subsequently sequenced using the BGISEQ-500 platform at the Beijing Genomics Institute. The raw scRNA-seq dataset consisted of i7 index reads, Read1 and Read2. Read1 contained 16 bp 10 \times Barcode and 10 bp UMI sequences. Read2 was used to detect the 98 bp cDNA fragments.

Pre-processing of raw scRNA-seq data

The reference genome and gene annotation files of *P. patens* were downloaded from JGI database Phytozome v13 (<https://phytozome-next.jgi.doe.gov/>). The raw scRNA-seq dataset was first analyzed by Cellranger v.3.1.0 (10 \times Genomics). A genomic reference was built by running ‘cellranger mkref’ with ‘–genome, –fasta and –genes’, and the expression matrix was generated by running ‘cellranger count’ with ‘–id, –transcriptome, –fastqs, –sample, and –chemistry = SC3Pv3’. The gene-cell matrices (named ‘filtered_gene_bc_matrices’, containing ‘barcodes.tsv.gz’, ‘features.tsv.gz’ and ‘matrix.tsv.gz’) were loaded into the Seurat v4.3.0 package for downstream analyses.⁷²

Cell clustering by nonlinear dimensional reduction

Low-quality cells (such as doublets and dead cells) and genes were filtered according to the following three criteria: a) cells with an expressed gene count higher than 8000 or less than 500 were removed; b) genes with expression in less than three cells were removed; c) cells with more than 10% mitochondrial sequences were removed. Subsequently, the scaled data were normalized using the ‘LogNormalize’, and principal component (PC) analysis was performed by reducing the ratio data to about 100 PCs based on the 2000 most variable genes. Cell clusters were identified using the Seurat function FindClusters with resolution 0.6. The data structure and cell locus were respectively determined by t-SNE (running RunTSNE function at dims = 20) and UMAP (n.neighbors = 30) visualization and exploration.^{75,76} CEGs were identified by Seurat FindAllMarkers and ROC with parameters set to min.pct = 0.25, log₂FC = 0.58 (above 1.5-fold difference), and p < 0.01.⁷⁷ Genes in each cluster were then used for GO annotation using clusterProfiler v4.0 and EggNOG v5.0.^{70,71} Finally, the WGCNA assay was conducted using the hdWGCNA R package (v.0.2.16) to identify the co-expressed genes.⁵⁶

Pseudotime analysis

Clusters 1, 5, and 6 from the filtered data were selected for pseudotime analysis. The Monocle v2.26.0 package was employed for trajectory analysis as previously described.^{36,37} This tool utilizes reversed graph embedding to arrange cell clusters in “pseudotime” order, providing an unsupervised depiction of their fate decisions. To identify pseudotime-related genes, the ‘differentialGeneTest’ function parameter was set to ‘q < 0.01’. The Branched Expression Analysis Modeling (BEAM) heatmap analysis was performed with ‘plot genes branched heatmap’ function, with ‘num clusters’ set to 5 and ‘q < 1e⁻⁴’.

Plasmid construction

For reporter assays, representative genes were selected based on their specific enrichment in clusters 0–6 (p < 0.001, and fold change greater than 1.8). Promoters (upstream of the start codon) of *JMJD5* (Pp3c2_7150, 1951 bp), *CRPK1* (Pp3c16_17510, 2114 bp), *EYA* (Pp3c1_31250, 2136 bp), *OST1* (Pp3c5_21160, 2118 bp), *KUP3* (Pp3c22_12740, 2160 bp), *PSBO2-1*

(Pp3c3_14080, 1968 bp), and *PHT2;1* (Pp3c16_25600, 2096 bp) were PCR-amplified from genomic DNA and fused into the *EcoRI* and *Sall* sites of pPro-EGFP vector using One Step Cloning Kit (Vazyme). See [Table S12](#) for primer details. After verification, these plasmids were linearized and separately introduced into WT plants.

For *pGmGH3::EGFP*, the promoter of *GmGH3* was obtained from a previous study⁵⁵ and biosynthesized into the *EcoRI* and *Sall* sites of pUC57 (Thermo Scientific) by Tsingke Biotechnology Co., Ltd. This sequence was amplified using the primers listed in [Table S12](#) and cloned into the pPro-EGFP with One Step Cloning Kit (Vazyme). After verification, this plasmid was linearized and separately introduced into WT and *βcaq#7* plants.

For *pβCA2pro::βCA2-EGFP*, the 2.2 kb promoter sequence and 753 bp coding regions (lacking the stop codon) of *βCA2* gene were amplified from genomic DNA and cDNA derived from WT plants using the primer pairs listed in [Table S12](#), respectively. The amplified fragments were cloned by sequential into the pPro-EGFP using sites *EcoRI/Sall* and *Sall* with One Step Cloning Kit (Vazyme). Similarly, the fragments of *βCA3* and *βCA6* genes were also amplified to construct *pβCA3pro::βCA3-EGFP* and *pβCA6pro::βCA6-EGFP* using the primer pairs listed in [Table S12](#), respectively. After verification, these plasmids were linearized and separately introduced into WT plants.

For *pU6::crRNA-βCAs*, the guide sequences of *βCAs* were designed using a web tool CRISPR-P v2.0 and then inserted into the vector pU6sgRNA using *Ncol* and *XbaI* sites according to methods previously described.^{62,73,78} For multiple gene editing, the three plasmids including 10 µg of pActLbCas12a (expressing RNA-guided endonucleases), 8 µg of pBNRF (expressing *nptII* resistance gene), and 12 µg of pU6crRNA-*βCAs* were co-delivered into WT plants.

PEG-mediated transformation

Plants were repeatedly crushed and inoculated on cellophane-overlaid BCDAT medium to produce chloronema-rich protonemata at 25°C. Collect the three- to five-day-old protonemal tissues for protoplast preparation (see above). Subsequently, the PEG-mediated transformation and resistant screening were completed as previously described.^{79,80} Briefly, 300 µL protoplast solution was gently mixed with 30 µL linearized plasmids and 300 µL PEG buffer (0.1 M Calcium nitrate, 10 mM Tris-HCl pH 8.0, 0.4 M D-Mannitol, and 40% PEG). The transformation mixture was heat shocked at 45°C for 5 min and then incubated at 20°C for 10 min. Subsequently, the mixture was gently mixed with 0.3, 0.6, 0.9, 1, and 3 mL of 8% D-Mannitol sequentially to recover the protoplasts, before being centrifuged at 800 rpm for 10 min at 25°C. After removing the supernatant and resuspending the pellets in 0.5 mL 8% D-Mannitol, 10 mL of top agar (preheating in the 42°C water bath) was added and poured the protoplast solution into cellophane-overlaid B medium. The protoplasts were regenerated on the B medium for a five-day incubation and were selected for successful transformants with 20 mg/L hygromycin B or geneticin (G418) for 3 weeks. Stable transformants were genotyped ([Figures S18, S20, and S21](#)).

Real-time quantitative PCR

Total mRNA was extracted from treated plants using a FastPure Universal Plant Total RNA Isolation Kit (Vazyme). First-strand cDNA synthesis and Real-Time quantitative PCR (RT-qPCR) were performed using a PerfectStart Uni RT&qPCR Kit (Transgen). Gene expression analysis was carried out with a Bio-Rad CFX96 Detection System. The thermal cycling profile was used as follows: 94°C for 30 s, 40 cycles of 94°C for 5 s, 57°C for 15 s, and 72°C for 10 s. The *ACT7* (Pp3c3_33410) and *EF1alpha* (Pp3c2_10310) were used for constitutive reference gene control.¹⁹ Specific sequences for primer pairs were listed in [Table S12](#).

Microscopy

GFP signals from reporter plants were visualized using a SZX7 stereo fluorescence microscope (Olympus). Phenotypes of these plants in bright-field were captured with an M165 stereomicroscope (Leica).

QUANTIFICATION AND STATISTICAL ANALYSIS

Statistical tests were performed using GraphPad Prism (<https://www.graphpad.com/>) or R program. Comparison of scRNA-seq data was performed using a Wilcoxon rank-sum test. Analysis of gene-gene correlation was performed using a Pearson correlation coefficient. The fluorescence intensity of GFP signal was quantified with ImageJ software. Two-tailed Student's t test was used to compare the means for two groups. A *p* value < 0.05 indicated statistical significance. Details about the statistically significant differences are described in the text or figure legends.